Cavity-State Coded Radar: A Simulation-Led Feasibility Study of Reconfigurable Electromagnetic State Diversity and DORT-Based Focused Interrogation

Andrew J. Wileman, N. Seddon

***Abstract*—This paper introduces cavity-state coded radar, a simulation-led concept in which a reconfigurable electromagnetic cavity provides an additional calibrated diversity dimension for radar sensing. Instead of relying only on time, frequency, phase, polarization, or a multi-element spatial aperture, the proposed architecture transmits a wideband radar waveform through a cavity-fed horn whose internal boundary conditions are changed by discrete stirrer states. Each state produces a repeatable complex electromagnetic response, allowing the received scene to be represented as a frequency-state data matrix. A hybrid CST/MATLAB modelling framework is developed to assess the feasibility of this approach. CST-derived near-field data from a cavity-fed horn are used to estimate state-dependent radiated-power weights, phase references, and angular pattern diversity, while MATLAB is used to model the wideband cavity response, target return, clutter, noise, regularised time-reversal calibration, range processing, and DORT-based mode extraction. The resulting formulation enables the dominant target-coupled scattering mode to be identified from the calibrated frequency-state matrix, and provides state- and frequency-importance measures for focused interrogation. Representative simulations over a 4–5 GHz bandwidth show that full DORT processing correctly estimates target range across several link-budget cases, while a reduced interrogation mode using selected cavity states and frequency bins preserves the range estimate with an approximately 75-85% reduction in processed frequency-state samples. The results suggest that cavity-state coding may offer a useful route to adaptive radar sensing in congested electromagnetic environments by shifting part of the diversity and resource-management problem into a calibrated electromagnetic state space.**

***Index Terms*—radar, DORT, electromagnetic state diversity, reconfigurable radar, time reversal, radar signal processing, cognitive radar, congested electromagnetic environments**

I. INTRODUCTION

RADAR systems are increasingly required to operate in electromagnetically congested, cluttered, and dynamically changing environments. Spectrum sharing with communications systems, the proliferation of active RF emitters, multipath-rich urban and indoor propagation, and the need for low-latency sensing all place pressure on conventional radar architectures. In response, modern radar research has explored a range of adaptive and diversity-based strategies, including waveform agility, cognitive radar, MIMO radar, adaptive beamforming, spectrum-aware sensing, and radar resource management [1] – [4]. These approaches seek to improve detection, localization, and imaging performance by exploiting additional degrees of freedom in time, frequency, waveform, polarization, aperture position, or spatial channel. However, many of these methods require large instantaneous bandwidths, multiple RF chains, high-speed beam steering, complex synchronization, or dense antenna apertures. This motivates continued interest in radar architectures that can generate useful measurement diversity with reduced hardware complexity.

One important line of work has therefore considered the use of coded and reconfigurable apertures as a means of replacing some of the burden of conventional spatial sampling with computational post-processing. Coded aperture radar has shown that spatial information can be encoded through aperture states, enabling range, velocity, and bearing estimation from a simplified single-transceiver architecture, albeit with trade-offs in received energy, SNR, and residual ambiguity [5]. More recently, reconfigurable intelligent surfaces and programmable coded apertures have been investigated for radar imaging with reduced RF-channel count, where different phase profiles or masks generate distinct observations of the scene and compressive reconstruction is used to recover target structure [6]. Dynamic meta-surface apertures extend this idea by using electronically tunable radiating elements to generate diverse radiation patterns from a compact aperture. In such systems, the sensing matrix, its singular-value spectrum, and the diversity of the radiated masks determine the information content available for reconstruction [7]. Frequency-diverse meta-surface antennas offer a related route, producing spatially incoherent radiation patterns as a function of frequency and enabling single-channel or reduced-channel computational imaging, including through-wall scenarios when appropriate clutter removal is applied [8].

These developments show that radar and microwave imaging systems need not rely solely on one-to-one spatial sampling by a conventional array. Instead, the aperture itself may be designed to encode the scene through a sequence of known electromagnetic states. Nevertheless, much of the coded-aperture and dynamic-meta-surface literature is directed toward image reconstruction, compressive sensing, or computational microwave imaging. The present work addresses a different but related question: whether a reconfigurable reverberant cavity

can be used as a calibrated electromagnetic state generator for radar interrogation, and whether the resulting state diversity can be processed using time-reversal and DORT principles to identify target-coupled modes and reduce the interrogation burden.

Time reversal provides a natural theoretical framework for exploiting complex propagation rather than treating it purely as a nuisance. In reciprocal and sufficiently stable media, a received waveform can be time reversed, or equivalently phase conjugated in the frequency domain, and backpropagated through the same channel to refocus energy at the original source or scattering location [9]. The decomposition of the time-reversal operator (DORT) extends this idea by using the eigensystem or singular-value structure of a measured propagation operator to identify coherent scattering modes. The original acoustic DORT work showed that individual scatterers in a multiple-scatterer medium can be associated with distinct eigenmodes of the time-reversal operator, enabling detection and selective focusing [10] – [12]. Subsequent work transferred this concept into electromagnetic scattering, establishing that DORT was not merely an acoustic technique but a more general wave-based method for extracting and focusing on scatterer-associated modes [13].

In electromagnetic radar and sensing, DORT and related time-reversal methods have been applied to buried-object detection, obscured-target imaging, cluttered environments, multi-static radar data, and ultrawideband imaging. Micolau, Saillard, and Borderies applied DORT to ultrawideband electromagnetic detection of buried objects, showing its value for scatterer detection, selective focusing, and clutter reduction [14]. Devaney formulated time-reversal imaging of obscured targets from multi-static data using the singular value decomposition of the multi-static data matrix, connecting the singular vectors to target localization through the background Green function [15]. Liu et al. experimentally demonstrated electromagnetic time-reversal imaging of a target in a cluttered environment, showing that accounting for the cluttered background can improve focusing relative to conventional imaging [16]. These works establish the central point that, when the propagation environment is sufficiently characterized, complex multipath and cluttered propagation can provide useful information rather than only degradation.

Time-reversal radar has also been studied from a detection and waveform-adaptation perspective. Jin and Moura developed time-reversal detection using antenna arrays and showed, with both analysis and electromagnetic measurements, that time reversal can provide detection gain over conventional approaches in multipath scattering environments [17]. Time-reversal MIMO radar further demonstrated how multipath can be used to enhance target detectability by matching the transmitted waveforms to the propagation medium and target scattering characteristics [18]. Later multi-static and distributed-MIMO formulations extended this idea to radar networks and multipath-clutter environments, including power-allocation strategies and moving-target cases where channel variation must be considered [19] – [21]. These studies are important for the present work because they show that multipath may be exploited when it is stable, estimated, or incorporated into the detection model. They also indicate a key limitation: uncontrolled environmental multipath can produce channel mismatch, clutter modes, or loss of focusing when the scene changes.

Several recent DORT-related works have further relaxed the conventional requirement for a fully populated multi-static array. Frequency-domain and space-frequency formulations have shown that the time-reversal operator need not always be constructed from a classical transmit-receive space-space matrix [22], [23]. Sakamoto proposed a stepped-frequency DORT method for a single-antenna ultrawideband radar in a known multipath environment, forming a frequency-frequency matrix and applying singular value decomposition to recover target information [24]. This is particularly relevant because it demonstrates that DORT can be reformulated around a nontraditional measurement matrix when the radar exploits a structured propagation environment. In that case, the additional diversity is provided by multipath and frequency sampling. In the present work, we instead introduce a deliberately reconfigurable electromagnetic state dimension generated by the radar front end itself.

The concept investigated here is cavity-state coded radar. A wideband radar waveform is transmitted through a cavity-fed horn, where a mechanically reconfigurable reverberant cavity produces a set of repeatable internal electromagnetic states. Each cavity state modifies the complex amplitude, phase, and angular radiation characteristics of the transmitted field. Rather than treating this state dependence as an implementation imperfection, the proposed architecture treats the cavity state as an explicit radar coding dimension. The received scene is therefore represented not only as a function of frequency, but as a frequency-state data matrix. This matrix can be calibrated, processed by regularized time reversal, and decomposed using DORT to identify target-coupled scattering modes.

This approach differs from prior coded-aperture and meta-surface radar work in that the coded measurement states are produced by the modal response of a reverberant cavity rather than by a large number of independently controlled aperture elements. It also differs from conventional time-reversal radar in that part of the propagation complexity is deliberately generated inside the radar front end, where it is repeatable and calibratable, rather than relying only on uncontrolled external multipath. The proposed architecture therefore occupies a position between reconfigurable computational apertures, time-reversal radar, and DORT-based coherent-mode extraction. It seeks to shift part of the radar diversity problem into a calibrated electromagnetic state space. The purpose of this paper is to present a simulation-led feasibility study of this concept.

A hybrid CST/MATLAB framework is developed in which CST-derived cavity-fed aperture data provide state-dependent radiation weights, phase references, and pattern diversity, while MATLAB is used to model the wideband cavity response, target return, noise, clutter, regularized time-reversal calibration, range processing, DORT decomposition, and reduced focused interrogation. The work is not presented as a

completed experimental radar demonstration. Rather, it asks whether the proposed frequency-state architecture is physically and algorithmically plausible, whether the dominant target-coupled mode can be extracted from the calibrated data matrix, and whether selected states and frequency bins can preserve the range estimate while reducing the processed measurement burden.

The main contributions of this paper are fourfold. First, a cavity-state coded radar architecture is proposed in which a reconfigurable reverberant cavity provides an additional calibrated electromagnetic diversity dimension for radar sensing. Second, a frequency-state signal model is developed in which the received scene is represented as a matrix indexed by frequency and cavity state. Third, a hybrid CST/MATLAB simulation framework is presented, combining full-wave cavity-fed aperture information with wideband radar propagation, clutter, noise, and regularized time-reversal calibration. Fourth, a DORT-based focused interrogation method is introduced to identify the cavity states and frequency bins most strongly coupled to the target response, enabling reduced interrogation while preserving the target range estimate in representative simulations.

The remainder of the paper is organized as follows. Section II introduces the cavity-state coded radar concept and the frequency-state measurement model. Section III describes the reconfigurable cavity-fed horn architecture and the CST-derived electromagnetic state data. Section IV presents the regularized time-reversal and DORT processing framework. Section V describes the simulation methodology and representative radar scenarios. Section VI presents full and reduced-interrogation results. Section VII discusses limitations, including calibration sensitivity, external multipath, clutter, moving-target coherence, and experimental validation requirements. Section VIII concludes the paper.

II. CAVITY-STATE CODED RADAR CONCEPT

A. Architectural Principle

The proposed radar architecture is based on the premise that a reconfigurable reverberant cavity can provide a repeatable electromagnetic state space for radar sensing. In a conventional radar front end, the antenna is normally designed to provide a stable radiation response, while measurement diversity is introduced through waveform design, frequency agility, polarization, spatial sampling, or multiple transmit and receive channels [25]. The proposed architecture instead introduces a deliberately state-dependent response into the radar front end.

As illustrated in Fig. 1, a wideband waveform excites a reverberant cavity that feeds a horn or other radiating aperture. An internal stirrer, movable perturbation, switched metallic inclusion, or electronically tunable boundary defines the cavity state. Changing this state modifies the interference among the cavity modes and therefore changes the complex field coupled into the aperture. Each state may consequently produce a different amplitude response, phase response, frequency dependence, and angular radiation pattern.

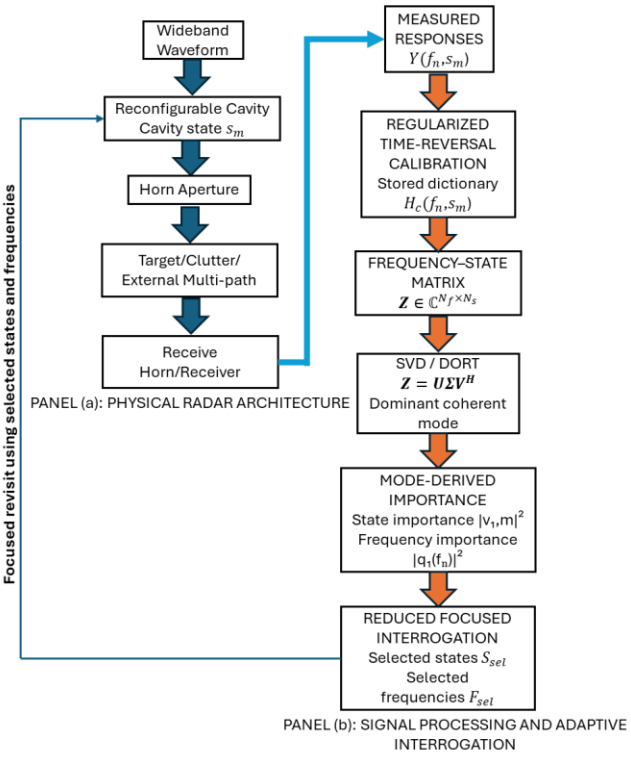


Fig. 1. Conceptual architecture and operating principle of cavity-state coded radar. (a) A wideband waveform is transmitted through a reconfigurable reverberant cavity whose state modifies the complex response and radiated field of the horn aperture. The target, clutter, and external-multipath returns are recorded over frequency and cavity state. (b) The measured responses are regularized using the stored cavity-state calibration dictionary and arranged as a frequency-state matrix. SVD/DORT processing identifies the dominant coherent mode and ranks the contributing cavity states and frequency samples, enabling reduced focused interrogation and subsequent target-dependent revisits.

The cavity states are not treated as uncontrolled implementation variations. Provided that they are sufficiently repeatable and can be calibrated, they form a set of known electromagnetic measurement states. The cavity therefore acts as a modal mixing structure that generates a coded measurement basis without requiring each radiated state to be produced by an independently controlled antenna element.

B. Frequency-State Measurement Concept

The transmitted bandwidth is sampled at a set of discrete frequencies, while the cavity is operated over a set of discrete states. For each combination of frequency and cavity state, the radar records a complex scene response. The complete measurement can therefore be arranged as a frequency-state matrix whose rows represent frequency samples and whose columns represent cavity states.

The frequency dimension contains the phase progression required for range estimation. The state dimension records how the target, clutter, and external propagation environment couple to the different calibrated electromagnetic states. A coherent target is therefore expected to produce structure across both dimensions: a repeatable progression over frequency and a characteristic coupling pattern over cavity state.

Before this structure can be interpreted, the known cavity

response must be compensated using a stored calibration dictionary. The purpose of this calibration is not to eliminate all state dependence. Rather, it removes the known first-order response of the cavity while retaining the state-dependent interaction between the radiated fields and the external scene. The resulting calibrated matrix is the principal data object used by the DORT processing developed in Section IV.

C. Broad Search and Focused Interrogation

The proposed operating sequence contains two stages. During broad search, the radar measures the scene using all, or a substantial subset, of the available frequencies and cavity states. Singular value decomposition is then used to identify coherent modes within the calibrated frequency-state matrix. A dominant target-coupled mode is characterized by its strength, its frequency-domain structure, and its cavity-state weighting.

The right singular vector associated with the selected mode indicates how strongly the individual cavity states contribute to that mode. The corresponding focused frequency response indicates which frequency samples provide the strongest coherent contribution. These quantities provide target-dependent measures of state and frequency importance.

During focused interrogation, the radar retains the most informative cavity states and frequency samples rather than repeating the complete broad-search measurement. The reduced measurement set can then be used for continued range estimation or subsequent revisits, provided that the selected subset preserves the target-coupled response. This creates a search-to-focused-interrogation sequence in which the cavity generates electromagnetic diversity, calibration makes that diversity usable, and DORT identifies the part of the measurement space most relevant to the detected target.

This operation should not be interpreted as conventional phased-array beam steering. The physical horn continues to determine the broad radiation envelope. The cavity-state and DORT processing instead provide a calibrated computational weighting of the electromagnetic states observed by the radar.

D. Scope of the Concept Study

The present work is a simulation-led feasibility study rather than a completed experimental radar demonstration. It examines whether CST-derived cavity-state information, combined with a plausible wideband cavity model, can produce a structured frequency-state response from which DORT can recover a target range and identify a reduced measurement subset.

The study assumes that the cavity states and target scene remain sufficiently stable during acquisition and that the stored calibration remains representative of the radar front end. The detailed signal model, regularized calibration, DORT formulation, and measurement-load metrics are developed in Section IV. The electromagnetic state characterization is presented first in Section III.

III. RECONFIGURABLE CAVITY-FED APERTURE AND ELECTROMAGNETIC STATE CHARACTERIZATION

A. Physical Configuration and Definition of the Cavity States

The electromagnetic front end consists of a metallic reverberant cavity feeding a wideband horn aperture. The representative geometry used in this study has internal cavity dimensions of 530 mm × 450 mm × 380 mm, corresponding to a volume of approximately 0.0906 m³. The horn provides the transition from the cavity to free space, with an approximate throat aperture of 180 mm × 120 mm, a mouth aperture of 500 mm × 400 mm, and a side length of approximately 280 mm. An approximate horn gain of 16 dBi is used in the subsequent radar model over the 4–5 GHz operating band.

An internal metallic stirrer perturbs the cavity boundary conditions [26]. Seven discrete stirrer angles are considered: 0°, 30°, 60°, 90°, 120°, 150°, and 180°. Each angle defines a cavity state, denoted by s_m. Changing the stirrer angle modifies the phase relationships among the excited cavity modes and therefore changes the complex field coupled into the horn aperture. The state change is consequently expected to affect four related quantities: the internal cavity field distribution, the amplitude response, the phase response, and the angular radiation pattern.

Although the angular sweep includes both 0° and 180°, these positions are not geometrically equivalent for the asymmetric stirrer assembly used in the CST model. The assembly is not invariant under a 180° rotation about its shaft; consequently, a half-turn relocates the conducting perturbation within the cavity and modifies the modal boundary conditions. The two endpoint positions are therefore retained as separate candidate states, with their electromagnetic distinctness assessed from the normalized complex-field and dictionary correlations rather than inferred from angular separation alone.

In a physical system, use of stirrer position as a code state will require the corresponding complex transfer function to remain repeatable under mechanical, thermal, and power variations.

TABLE I
REPRESENTIVE ELECTROMAGNETIC FRONT-END PARAMETERS

Parameter	Value or description
Operating band	4–5 GHz
Reference CST field frequency	4.5 GHz
Cavity internal dimensions	530 mm × 450 mm × 380 mm
Cavity volume	0.0906 m³
Horn throat	Approximately 180 mm × 120 mm
Horn mouth	Approximately 500 mm × 400 mm
Horn side length	Approximately 280 mm
Approximate horn gain	16 dBi
Cavity states	0° to 180° in 30° increments
Number of states	7
CST field-monitor plane	$z = 761.5$ mm in the model coordinate system

B. CST Full-Wave Characterization and Field Sampling

A full end-to-end electromagnetic simulation containing the cavity, horn, long free-space propagation region, target, clutter, receiver, and every stirrer state would be computationally prohibitive at operational radar ranges. The electromagnetic

subsystem is therefore characterized locally in CST. The full-wave model contains the feed, cavity, stirrer, and horn, while the radiated complex fields are sampled on a transverse plane in front of the horn.

For each stirrer state, the Cartesian electric- and magnetic-field components are exported on a common rectangular grid at the 4.5 GHz reference frequency. The exported data comprise the real and imaginary parts of E_x, E_y, E_z, H_x, H_y, and H_z. These components are reconstructed as complex phasors and checked for common spatial sampling before any state-dependent quantities are calculated.

The monitor plane provides three forms of information. First, the electric and magnetic fields permit estimation of the forward power associated with each state. Second, the complex electric field provides a consistent phase reference. Third, the transverse field distribution acts as an equivalent aperture field from which relative angular-pattern differences can be estimated. The complete complex field maps are retained; the scalar power and phase weights introduced below are only compact first-order summaries used to anchor the wideband model.

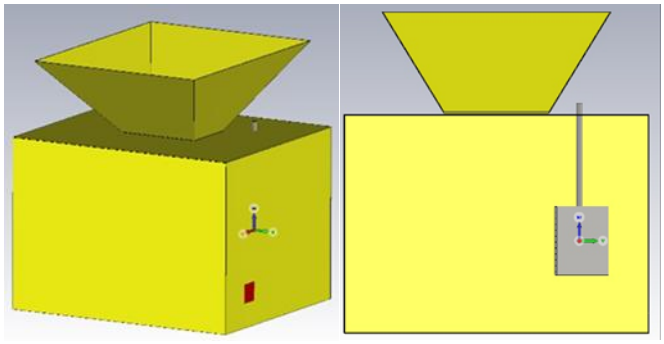


Fig. 2. CST model of the reconfigurable cavity-fed horn shown in oblique and side views. The internal feed and movable metallic perturbation modify the cavity modal field before coupling into the horn aperture.

C. State-Dependent Radiated Power and Phase Reference

For the mth cavity state, the time-averaged complex Poynting vector on the monitor plane is

$$\mathbf{S}_m(x,y) = \frac{1}{2}\mathbf{E}_m(x,y) \times \mathbf{H}_m^*(x,y) \qquad (1)$$

Here, the superscript asterisk denotes complex conjugation. If the monitor plane normal is $\hat{\mathbf{n}}$, the forward radiated power used in the present model is estimated from the positive real normal power flow,

$$P_m = \iint_A \max\{\mathrm{Re}[\mathbf{S}_m(x,y)\cdot\hat{\mathbf{n}}], 0\}\,\mathrm{d}A \qquad (2)$$

Using only the positive normal component prevents local reactive or backward-flow regions on the finite monitor plane from cancelling the forward-flow estimate. This quantity is used as a relative state metric rather than as a substitute for a rigorously calibrated total radiated-power measurement.

Because the radar signal model is expressed in complex field or voltage amplitude, the normalized amplitude weight is obtained from the square root of the power ratio,

$$a_m = \sqrt{\frac{P_m}{\max_q P_q}} \qquad (3)$$

A state phase reference is extracted from a selected electric-field component close to the center of the monitor plane,

$$\phi_m = \arg\{E_{\mathrm{ref},m}(x_0,y_0)\} \qquad (4)$$

The resulting complex state weight is

$$w_m = a_m \exp(j\phi_m) \qquad (5)$$

The weight w_m captures the first-order relative amplitude and phase difference among the stirrer states at the reference frequency. It does not contain the full spatial information in the aperture field. In an experimental implementation, the reference point should be chosen away from a deep field null; a spatially weighted coherent average could also be used to improve robustness to local measurement noise.

D. Near-Field and Angular Pattern Diversity

The usefulness of cavity-state coding depends on more than a change in total transmitted power. If two states differ only by a scalar gain or common phase, they provide limited additional spatial information. The complex field maps should therefore be compared directly. Let $\mathbf{e}_m$ denote a vector formed by stacking the sampled transverse electric-field components for state m. A normalized pairwise field correlation may be defined as

$$\rho_{pq} = \frac{|\mathbf{e}_p^H \mathbf{e}_q|}{\|\mathbf{e}_p\|_2 \|\mathbf{e}_q\|_2}, \qquad 0 \le \rho_{pq} \le 1 \qquad (6)$$

A value close to unity indicates that two complex field maps are nearly identical apart from a scalar factor, whereas a lower value indicates greater spatial-state diversity. The complete correlation matrix and the singular values of the stacked state-field matrix provide useful quantitative checks on the number of independently informative states. These quantities should be reported alongside visual field maps in the results section rather than relying on visual differences alone.

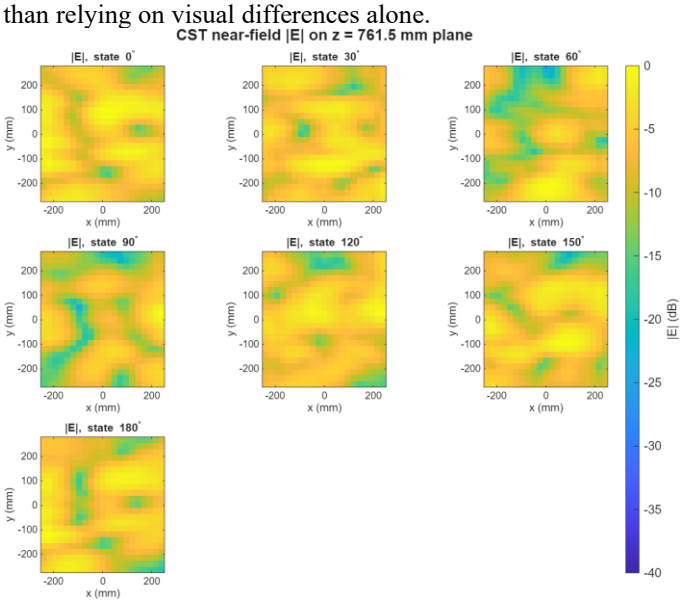


Fig. 3. Normalized CST near-field magnitude $|E|$ on the $z =$ 761.5 mm monitor plane at 4.5 GHz for the seven cavity stirrer states. The

changing spatial distributions demonstrate that each stirrer position produces a distinct electromagnetic aperture state.

To estimate relative angular diversity, the transverse fields on the monitor plane are treated as an equivalent aperture distribution [27]. After applying a two-dimensional Hann window $W(x,y)$ to reduce truncation discontinuities, the plane-wave spectra are approximated by

$$\tilde{E}_{\alpha,m}(k_x,k_y)=\iint_A W(x,y)E_{\alpha,m}(x,y)\exp\left[-j\left(k_x x+k_y y\right)\right]\mathrm{d}x\,\mathrm{d}y,\quad \alpha\in\{x,y\} \tag{7}$$

The transverse wavenumbers are mapped to direction cosines $u=k_x/k_0$ and $v=k_y/k_0$, where $k_0=2\pi f_0/c$. Only the visible region $u^2+v^2\le 1$ is retained. A relative angular power pattern is then formed as

$$G_m(u,v)\propto\left|\tilde{E}_{x,m}(u,v)\right|^2+\left|\tilde{E}_{y,m}(u,v)\right|^2, \tag{8}$$

and normalized to the maximum value before conversion to decibels.

This Fourier-transform procedure is used to compare the angular behaviour of the states; it is not claimed to replace a rigorous calibrated near-field-to-far-field transformation or a full CST far-field solution. The finite monitor-plane extent, field truncation, sampling density, polarization treatment, and distance from the physical aperture all affect the result. Accordingly, the derived patterns are interpreted as relative state-dependent pattern estimates rather than absolute gain predictions. Their role is to demonstrate that the cavity states provide an angular component of diversity in addition to scalar power and phase variation.

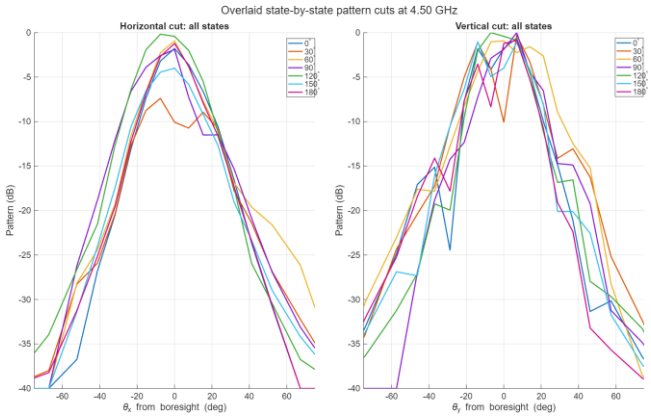


Fig. 4. Normalized horizontal and vertical far-field pattern cuts at 4.5 GHz for the seven cavity stirrer states. Although the general horn beam is retained, the stirrer states produce measurable changes in peak direction, beam shape, null locations, and sidelobe structure, demonstrating a spatial component to the cavity-state electromagnetic diversity

E. Construction of the Wideband Cavity-State Calibration Dictionary

The CST field data characterize the states at the 4.5 GHz reference frequency, whereas the radar model operates across the complete 4–5 GHz band. A wideband complex response must therefore be assigned to every state. In the present feasibility model, the CST-derived weight anchors a synthetic frequency-dependent reverberant response,

$$H_c(f,s_m)=w_m\,\overline{H}_m(f),\qquad \overline{H}_m(f_0)=1, \tag{9}$$

where $f_0=4.5$ GHz. The normalization condition ensures that the synthetic response preserves the CST-derived complex amplitude and phase at the reference frequency.

The number of physical cavity modes in the band may be estimated using the Weyl mode-count approximation [28]. The normalized wideband term is generated from a reduced modal representation,

$$\tilde{H}_m(f)=D_m(f)\sum_{\ell=1}^{L}b_{\ell m}\exp(-j2\pi f\tau_{\ell m})$$
$$\overline{H}_m(f)=\frac{\tilde{H}_m(f)}{\tilde{H}_m(f_0)} \tag{10}$$

Here, $b_{\ell m}$ and $\tau_{\ell m}$ are the complex amplitude and effective delay of the ℓth modal contribution in state m, and $D_m(f)$ represents broader deterministic ripple. The delayed complex contributions produce the amplitude ripple, phase rotation, constructive interference, destructive interference, and state-dependent nulls expected from a reverberant structure.

Sampling the wideband response over all frequencies and states forms the calibration dictionary

$$\mathbf{H}_c=[H_c(f_n,s_m)]\in\mathbb{C}^{N_f\times N_s} \tag{11}$$

The columns of this matrix are the wideband code responses associated with the cavity states. A normalized dictionary correlation matrix,

$$\mathbf{C}_H=\hat{\mathbf{H}}_c^H\hat{\mathbf{H}}_c \tag{12}$$

where each column of $\hat{\mathbf{H}}_c$ has unit norm, provides a second measure of state distinctness across the operating band. Large off-diagonal magnitudes indicate redundant state responses, while a better-conditioned dictionary with a broader singular-value spectrum indicates a richer measurement basis.

Only the 4.5 GHz state anchors are obtained directly from CST in the present study; the detailed 4–5 GHz modal response is synthetic. Measured wideband calibration is therefore required before operational performance can be assessed.

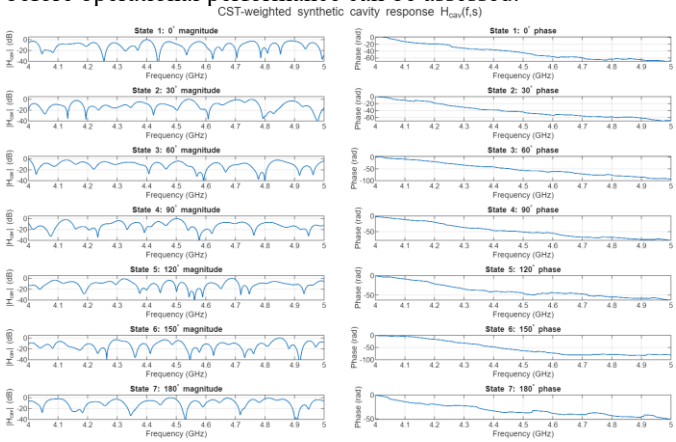


Fig. 5. CST-anchored synthetic wideband cavity responses over 4–5 GHz for the seven stirrer states. The left and right columns show the normalized

magnitude and unwrapped phase, respectively. Each response is constrained by the CST-derived complex state weight at the 4.5 GHz reference frequency and extended across the operating band using the reduced modal cavity model. The state-dependent spectral nulls and phase evolution provide the wideband diversity used to construct the calibration dictionary.

F. Conditions for a Useful Electromagnetic State Basis

A useful state basis must be repeatable, sufficiently distinct in complex response or radiation pattern, radiatively efficient enough to avoid severe noise amplification, and stable over the acquisition interval. The quantitative field-correlation and dictionary-conditioning measures introduced above provide tests of these requirements.

The CST characterization supports the physical plausibility of the concept by providing state-dependent complex fields, power weights, phase references, and relative angular patterns. The quantitative correlation and dictionary-conditioning measures defined above provide a route to testing whether the available seven-state set is genuinely informative rather than merely different in appearance. These characterized cavity states form the electromagnetic input to the radar-return, regularized calibration, and DORT processing model developed in Section IV.

IV. Radar Signal Model and DORT Processing

Section II described the proposed architecture and its search-to-focused-interrogation sequence qualitatively. This section formalizes the received-signal model, regularized cavity calibration, frequency-state matrix, DORT decomposition, and reduced-interrogation metrics used in the simulations.

A. Target, Clutter, Noise, and External-Multipath Model

For each sampled frequency and cavity state, the received signal is modelled as a superposition of coherent target returns, clutter components, possible external multipath terms, and receiver noise. Let the radar bandwidth be sampled at frequencies f_n, where $n = 1, \dots, N_f$, and let the cavity states be denoted by s_m, where $m = 1, \dots, N_s$. The measured complex return may be written as

$$Y(f_n, s_m) = Y_{\mathrm{tar}}(f_n, s_m) + Y_{\mathrm{clut}}(f_n, s_m) + Y_{\mathrm{mp}}(f_n, s_m) + W(f_n, s_m) \tag{13}$$

Here, Y_{tar} is the target contribution, Y_{clut} is the contribution from clutter scatterers, Y_{mp} represents external multipath components not contained inside the cavity calibration, and W is additive receiver noise. The internal cavity response is treated separately from external propagation because it is part of the calibrated radar front end. External multipath, by contrast, is produced by the scene and may be either useful or detrimental depending on its stability and coherence.

For a single dominant target at range R, the target contribution is modelled as

$$Y_{\mathrm{tar}}(f_n, s_m) = A_{\mathrm{tar}}(f_n)\, H_{\mathrm{c}}(f_n, s_m)\, \Gamma_{\mathrm{tar}}(f_n, s_m) \exp\left(-j\frac{4\pi f_n R}{c}\right) \tag{14}$$

In (14), $A_{\mathrm{tar}}(f_n)$ contains the radar-equation amplitude scaling, $H_{\mathrm{c}}(f_n, s_m)$ is the calibrated cavity-state response, $\Gamma_{\mathrm{tar}}(f_n, s_m)$ is an additional target coupling factor, and c is the speed of light. The exponential term represents the two-way propagation phase for a monostatic-equivalent range model. For a bistatic geometry, the phase term may be replaced by $\exp[-j2\pi f_n(R_{\mathrm{T}} + R_{\mathrm{R}})/c]$, where R_{T} and R_{R} are the transmitter-to-target and target-to-receiver path lengths.

The radar-equation amplitude term may be written in simplified bistatic form as [29]

$$P_{\mathrm{r}}(f_n) = \frac{P_{\mathrm{t}} G_{\mathrm{t}}(f_n) G_{\mathrm{r}}(f_n) \lambda_n^2 \sigma}{(4\pi)^3 R_{\mathrm{T}}^2 R_{\mathrm{R}}^2} \tag{15}$$

where P_{t} is transmit power, G_{t} and G_{r} are transmit and receive gains, $\lambda_n = c/f_n$, and σ is the radar cross-section. The corresponding complex-voltage amplitude is proportional to $\sqrt{P_{\mathrm{r}}(f_n)}$. In the simulation, the simplified amplitude model is sufficient because the principal objective is to test the effect of cavity-state diversity and DORT selection rather than to claim a final operational link budget.

For multiple point targets and clutter scatterers, the coherent scene response may be generalized as

$$Y_{\mathrm{scene}}(f_n, s_m) = \sum_{q=1}^{Q} A_q(f_n)\, H_{\mathrm{c}}(f_n, s_m)\, \Gamma_q(f_n, s_m) \exp\left(-j\frac{2\pi f_n L_q}{c}\right) \tag{16}$$

where Q is the number of target, clutter, or multipath components, A_q is the amplitude of the q-th component, Γ_q is its state-dependent coupling, and L_q is the total propagation path length. For a direct monostatic-equivalent target, $L_q = 2R_q$. For an external multipath path involving a building, wall, ground bounce, or other reflector, L_q represents the longer indirect path length. This form makes explicit that the cavity state can weight different propagation paths differently, because each path may couple to a different angular portion of the cavity-fed aperture pattern.

In the present simulation-led study, clutter and external multipath are represented in simplified form as additional weak coherent scatterers plus additive noise. This is sufficient to test whether the calibrated cavity-state response can support a dominant target-coupled mode. More realistic urban, indoor, or external multipath models would require measured or full-wave environmental channel data and are therefore treated as part of the experimental validation pathway.

B. Regularized Time-Reversal Calibration

The measured response in (14) includes the known state-dependent cavity transfer function. If this response were not compensated, the singular structure of the data matrix could be dominated by the cavity itself rather than by target-coupled scattering. The first processing step is therefore to calibrate the received data against the stored cavity response.

In the frequency domain, time reversal corresponds to complex conjugation. A regularized time-reversal calibration is applied to each frequency-state sample:

$$Z(f_n, s_m) = \frac{Y(f_n, s_m) H_{\mathrm{c}}^*(f_n, s_m)}{|H_{\mathrm{c}}(f_n, s_m)|^2 + \lambda} \tag{17}$$

The numerator phase-aligns the received signal with the stored cavity-state response. The denominator prevents numerical instability near cavity nulls, where a direct division by $H_c(f_n, s_m)$ would amplify noise and modelling error. The regularization parameter λ therefore controls the trade-off between cavity-response equalization and noise robustness. In practice, λ may be chosen as a small fraction of the mean or maximum value of $|H_c|^2$, or estimated from a measured noise floor.

The calibration in (17) should not be interpreted as removing all state dependence. Rather, it removes the known first-order cavity transfer function so that the remaining calibrated response contains the state-dependent coupling between the calibrated aperture states and the scene. This distinction is important: if the target, clutter, or external multipath components couple differently to the radiated states, that residual state structure is retained and becomes useful for DORT processing.

C. Frequency-State Matrix Construction

After calibration, the scalar samples $Z(f_n, s_m)$ are assembled into the frequency-state matrix

$$\mathbf{Z} = \begin{bmatrix} Z(f_1, s_1) & Z(f_1, s_2) & \cdots & Z(f_1, s_{N_s}) \\ Z(f_2, s_1) & Z(f_2, s_2) & \cdots & Z(f_2, s_{N_s}) \\ \vdots & \vdots & \ddots & \vdots \\ Z\left(f_{N_f}, s_1\right) & Z\left(f_{N_f}, s_2\right) & \cdots & Z\left(f_{N_f}, s_{N_s}\right) \end{bmatrix} \quad (18)$$

The rows of $\mathbf{Z}$ correspond to frequency samples and therefore contain range information through phase progression over frequency. The columns correspond to cavity states and therefore contain the electromagnetic state-coupling information introduced by the reconfigurable cavity-fed aperture. The matrix may be interpreted as a compact representation of how the scene responds to the calibrated frequency-state measurement basis.

For a scene dominated by a single target-coupled scattering mode, $\mathbf{Z}$ is expected to have a strong approximately low-rank component. In this case, the data may be expressed conceptually as

$$\mathbf{Z} = \mathbf{Z}_{\text{tar}} + \mathbf{Z}_{\text{res}} \quad (19)$$

where $\mathbf{Z}_{\text{tar}}$ is the structured target-coupled component and $\mathbf{Z}_{\text{res}}$ contains residual clutter, noise, modelling error, and weaker scattering components. The objective of DORT processing is to identify and extract the dominant coherent component from this matrix.

D. SVD/DORT Mode Extraction

The DORT step applies singular value decomposition to the calibrated frequency-state matrix:

$$\mathbf{Z} = \mathbf{U}\mathbf{\Sigma}\mathbf{V}^H \quad (20)$$

Equivalently, the right singular vectors diagonalize the state-space time-reversal operator $\mathbf{Z}^H\mathbf{Z} = \mathbf{V}\mathbf{\Sigma}^2\mathbf{V}^H$, while the left singular vectors diagonalize $\mathbf{Z}\mathbf{Z}^H = \mathbf{U}\mathbf{\Sigma}^2\mathbf{U}^H$. The SVD therefore implements the corresponding DORT eigendecomposition without explicitly forming either operator. Here, $\mathbf{U} \in \mathbb{C}^{N_f \times N_f}$ contains the left singular vectors, $\mathbf{V} \in \mathbb{C}^{N_s \times N_s}$ contains the right singular vectors, $\mathbf{\Sigma}$ contains the singular values, and $(\cdot)^H$ denotes Hermitian transpose. In the present radar formulation, the left singular vectors describe the frequency-domain structure of the extracted scattering modes, while the right singular vectors describe the corresponding cavity-state weighting. The singular values quantify the strength of each coherent mode.

The decomposition can be written as a modal expansion,

$$\mathbf{Z} = \sum_{k=1}^{K_{\text{svd}}} \sigma_k \, \mathbf{u}_k \mathbf{v}_k^H \quad (21)$$

where σ_k is the k-th singular value and $\mathbf{u}_k$, $\mathbf{v}_k$ are the associated frequency and cavity-state singular vectors. If the first singular value is well separated from the remaining singular values, the leading mode

$$\mathbf{Z}_1 = \sigma_1 \mathbf{u}_1 \mathbf{v}_1^H \quad (22)$$

may be interpreted as the dominant coherent scattering mode. In the intended operating regime, this mode is associated with the target-coupled response. However, the interpretation must be made carefully: the leading singular mode is the strongest coherent mode in the calibrated matrix, which may correspond to a target, a dominant clutter component, or a stable external multipath path if appropriate background subtraction or gating is not applied.

The DORT-focused frequency response is formed by projecting the calibrated matrix onto the dominant cavity-state vector:

$$P_{\text{DORT}}(f_n) = \sum_{m=1}^{N_s} Z\,(f_n, s_m) v_{1,m} \quad (23)$$

This operation coherently combines the cavity states using weights derived from the data rather than by uniform averaging. The resulting spectrum is therefore focused onto the dominant state-coupled mode. The range profile is then obtained by applying frequency-to-range processing, for example by an inverse discrete Fourier transform across the sampled bandwidth:

$$p_{\text{DORT}}(r) = \left| \sum_{n=1}^{N_f} w_n \, P_{\text{DORT}}(f_n) \exp\left(j \frac{4\pi f_n r}{c}\right) \right| \quad (24)$$

where w_n is a spectral window used to control sidelobes [30]. The estimated target range is obtained from the peak of $p_{\text{DORT}}(r)$.

E. State and Frequency Importance

The singular vectors provide a natural way to rank the information carried by different cavity states and frequency samples. The state importance of the m-th cavity state is defined from the leading right singular vector as

$$I_s(m) = \left| v_{1,m} \right|^2 \quad (25)$$

A large value of $I_s(m)$ indicates that state s_m contributes strongly to the dominant target-coupled mode. This does not

necessarily mean that the state radiates the most power overall; rather, it means that the state is strongly aligned with the coherent mode extracted by DORT.

Similarly, the frequency importance may be estimated from the focused spectrum as

$$I_f(n) = |P_{\mathrm{DORT}}(f_n)|^2 \tag{26}$$

A large value of $I_f(n)$ indicates that frequency sample f_n contributes strongly to the focused response. Together, $I_s(m)$ and $I_f(n)$ provide a practical mechanism for identifying which cavity states and frequency bins should be retained during subsequent focused interrogation.

Other importance metrics are possible. For example, one may average over several singular modes, reject modes associated with static clutter, or include constraints based on spectrum occupancy. The present paper uses the leading-mode definitions in (25) and (26) because they are simple, interpretable, and directly linked to the DORT-focused range response.

F. Focused Reduced Interrogation and Processing-Load Metric

The proposed operating sequence is intended to support a broad-search stage followed by a reduced focused-interrogation stage. In the broad-search stage, all available frequency samples and cavity states are used to form **Z**, apply DORT, and estimate the target range. The leading singular vectors are then used to select a smaller subset of informative states and frequency samples.

Let $\mathcal{S}' \subseteq \{s_1, \dots, s_{N_s}\}$ denote the selected cavity-state set and $\mathcal{F}' \subseteq \{f_1, \dots, f_{N_f}\}$ denote the selected frequency set. If $N_s{}' = |\mathcal{S}'|$ and $N_f{}' = |\mathcal{F}'|$, the reduced frequency-state matrix contains

$$N_{\mathrm{red}} = N_f{}' N_s{}' \tag{27}$$

processed samples, compared with

$$N_{\mathrm{full}} = N_f N_s \tag{28}$$

samples in the full search. The fractional processing load is therefore

$$\eta_{\mathrm{load}} = \frac{N_f{}' N_s{}'}{N_f N_s} \tag{29}$$

and the percentage reduction is

$$\eta_{\mathrm{red}} = 100\left(1 - \frac{N_f{}' N_s{}'}{N_f N_s}\right)\% \tag{30}$$

In the representative simulations, the reduced interrogation is evaluated by comparing the range estimate obtained from the reduced matrix with the range estimate obtained from the full matrix. A reduced interrogation is considered successful when the target range peak is preserved within the expected range-bin tolerance and when the focused response remains distinguishable from sidelobes, clutter leakage, and noise.

This reduced-interrogation metric is intentionally simple. It measures the number of processed frequency-state samples rather than the full computational cost of every operation. In practice, the system-level benefit may appear as reduced processing time, reduced spectral occupancy, reduced state-switching burden, or increased update rate. The precise operational benefit depends on how the radar waveform, cavity-state switching, receiver sampling, and digital processing are implemented. Nevertheless, the metric in (29) and (30) provides a transparent first-order way to quantify the reduction achieved by DORT-based state and frequency selection.

V. SIMULATION METHODOLOGY

A. Purpose and Modeling Boundary

The model uses a hybrid CST/MATLAB architecture. CST provides the complex electric- and magnetic-field data on the monitor plane for each of the seven stirrer states at the 4.5 GHz reference frequency. As described in Section III, these fields are used to estimate the relative radiated power, state phase reference, near-field diversity, and angular pattern associated with each state. They also provide the complex anchor used to construct the wideband cavity-state calibration dictionary.

MATLAB is then used to model the components outside the local CST electromagnetic domain: the synthetic 4–5 GHz cavity response, free-space propagation, target radar cross-section, weak clutter scatterers, receiver noise, regularized time-reversal calibration, frequency-to-range processing, SVD/DORT decomposition, and the selection of reduced frequency and state subsets. Full and reduced processing are applied to the same simulated scene realization unless otherwise stated, so that differences in performance are attributable to the selected measurement subset rather than to a change in the underlying target, clutter, or noise conditions.

The simulation is therefore not an end-to-end prediction of an operational radar. It is a controlled feasibility model that combines physically derived aperture-state information with a parameterized radar scene. Its purpose is to determine whether the proposed architecture behaves consistently across different ranges and link budgets, and to identify which assumptions require later experimental validation.

The computational sequence used for every scenario is:

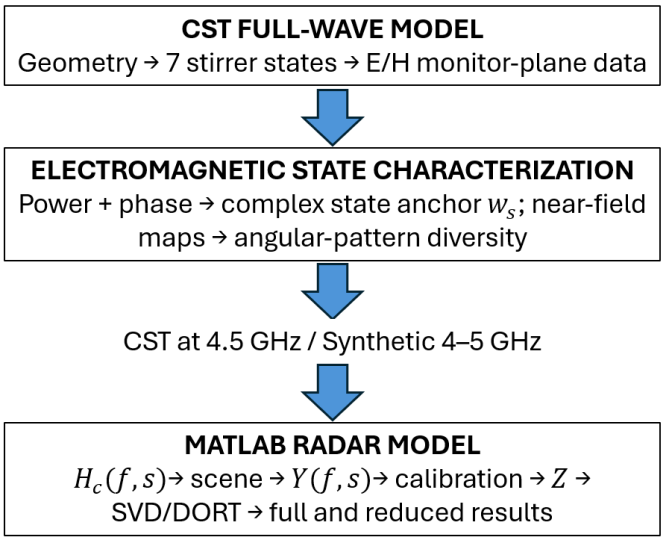


Fig. 6. Hybrid CST/MATLAB simulation methodology used to evaluate cavity-state coded radar. CST full-wave simulations provide complex electric- and

magnetic-field data for seven cavity stirrer states at the 4.5 GHz reference frequency. These data are used to obtain state-dependent power and phase information, complex state anchors, near-field distributions, and relative angular-pattern diversity. The CST-derived state anchors are then used to construct a synthetic wideband cavity-state dictionary over 4–5 GHz. MATLAB models the radar scene, received frequency-state response, regularized calibration, frequency-state matrix formation, SVD/DORT processing, state and frequency importance, and full and reduced-interrogation results.

B. Common Physical and Radar Parameters

The common parameters used throughout the representative simulations are summarized in Table II. The cavity and horn dimensions are reported in Table I and are not repeated here. Parameters associated with the target and link budget are varied by scenario.

TABLE II
Common Simulation Parameters

Parameter	Value or description
Operating band	4–5 GHz
Center frequency	4.5 GHz
Bandwidth	1 GHz
Nominal range resolution	0.15 m
Cavity states	0° to 180° in 30° increments
Number of cavity states, N_s	7
CST reference-field frequency	4.5 GHz
CST monitor plane	$z = 761.5$ mm in the model coordinate system
Approximate transmit horn gain	16 dBi
Approximate receive horn gain	16 dBi
Receiver noise floor	-100 dBm unless otherwise stated
Clutter	Optional weak coherent scatterers with random phases and range offsets
External multipath	Optional additional coherent paths represented by effective path lengths and state coupling
Target range, transmit power, and RCS	Scenario dependent
State-selection method	Leading right singular-vector importance
Frequency-selection method	DORT-focused spectral importance

The target range, transmit power, radar cross-section, clutter level, and frequency sampling are parameterized. This permits the same processing chain to be evaluated at laboratory scale, practical outdoor ranges, and deliberately stressed link-budget conditions. The values used here are representative test cases rather than claimed performance limits.

C. Frequency Sampling and Range Processing

The stepped-frequency representation spans the interval from $f_{\min} = 4$ GHz to $f_{\max} = 5$ GHz. The bandwidth is

$$B = f_{\max} - f_{\min} = 1 \text{ GHz} \tag{31}$$

For a wideband or stepped-frequency radar, the nominal two-way range resolution is [30]

$$\Delta R = \frac{c}{2B} \tag{32}$$

Using $B = 1$ GHz gives $\Delta R \approx 0.15$ m. This value is determined by the occupied bandwidth and is not improved by increasing the number of zero-padded inverse-transform points.
The frequency samples are uniformly spaced according to

$$f_n = f_{\min} + (n-1)\Delta f, \qquad n = 1, \dots, N_f \tag{33}$$

The frequency increment controls the monostatic-equivalent unambiguous range [30],

$$R_{\mathrm{u}} = \frac{c}{2\Delta f} \tag{34}$$

For each scenario, Δf is selected so that R_{u} exceeds the largest range of interest by a safety margin. If the required unambiguous range is written as $R_{\mathrm{req}} = \gamma R_{\max}$, where $\gamma > 1$, then

$$\Delta f \le \frac{c}{2\gamma R_{\max}} \tag{35}$$

The corresponding minimum number of frequency samples is

$$N_{f,\mathrm{req}} = 1 + \mathrm{ceil}\left(\frac{B}{\Delta f}\right) \tag{36}$$

In the implementation, the sample count is rounded upward to a convenient transform length, with a minimum of approximately 10^3 samples. Longer target ranges therefore require a smaller frequency step and a larger frequency-state matrix, while the physical range resolution remains fixed by the 1 GHz bandwidth.
After the DORT-focused spectrum has been formed, a Hann window is applied across frequency before the inverse discrete Fourier transform. The window reduces range sidelobes at the cost of a modest broadening of the main lobe. If an N_{FFT}-point transform is used, the displayed range-grid spacing is

$$\delta R_{\mathrm{grid}} = \frac{c}{2N_{\mathrm{FFT}}\Delta f} \tag{37}$$

When $N_{\mathrm{FFT}} > N_f$, zero padding provides a smoother interpolation of the range profile but does not change the resolution in (32). The target range estimate is taken from the maximum of the magnitude range profile within the unambiguous interval.

D. Representative Simulation Scenarios

Four representative scenarios are used to evaluate the processing chain as the propagation distance and link-budget difficulty increase. The cases are not intended to establish absolute detection limits. Instead, they provide a structured test of whether the target range and dominant mode remain recoverable and whether the reduced interrogation continues to preserve the full-search result.

TABLE III
Representative Simulation Scenarios

Scenario	Range	Transmit power	Target RCS	Clutter
A. Lab validation	10 m	1 W	1 m²	Yes
B. Outdoor target	100 m	10 W	1 m²	Yes

Scenario	Range	Transmit power	Target RCS	Clutter
C. 1 km target	1000 m	10 W	1 m²	Yes
D. 1 km stress case	1000 m	10 W	0.1 m²	Yes

Scenario A is linked to a controlled short-range validation geometry and checks that the complete CST-to-DORT processing chain behaves sensibly. Scenario B tests range recovery beyond the local CST domain under a practical outdoor link budget. Scenario C examines kilometer-range signal-processing feasibility for a comparatively favorable target. Scenario D reduces the target return by 10 dB relative to Scenario C to examine degradation and robustness.

All scenarios use the same cavity states, CST-derived state anchors, wideband modeling procedure, calibration, and DORT processing. The number of frequency samples changes where necessary to maintain an unambiguous range greater than the specified target distance. Clutter is represented by weaker returns placed at range offsets around the principal target, with independently assigned complex amplitudes and phases.

E. Evaluation Metrics and Comparison Procedure

The methodology evaluates more than the visibility of a range peak. The principal question is whether the frequency-state data contain a coherent target-coupled mode and whether that mode can be retained after reducing the measurement set.

The absolute range-estimation error is

$$\varepsilon_R = \left|\hat{R} - R_0\right| \tag{38}$$

where R_0 is the simulated target range and $\hat{R}$ is the range-profile peak. Separate errors are recorded for the full DORT result and the reduced-interrogation result.

The fraction of calibrated matrix energy contained in the leading singular mode is

$$\eta_1 = \frac{\sigma_1^2}{\sum_k \sigma_k^2} \tag{39}$$

A large value of η_1 indicates that the response is dominated by one coherent mode, although it does not by itself prove that the mode corresponds to the desired target. The singular-value spectrum is therefore interpreted alongside the known target range, range profiles, state importance, frequency importance, and clutter response.

The full and reduced results are compared using four primary criteria:

1. preservation of the target range peak within the expected range-bin tolerance;
2. preservation of a distinct dominant singular mode or target-focused response;
3. the number and identity of retained cavity states and frequency bins; and
4. the processing-load fraction and percentage reduction defined in (29) and (30).

Additional diagnostic plots include the range response for each individual stirrer state, the calibrated frequency-state magnitude map, the singular-value spectrum, state- and frequency-importance profiles, and the full- versus reduced-state angular-pattern comparison. These diagnostics are used to explain *why* the reduced selection succeeds or fails rather than being treated as independent detection metrics.

The initial all-state response, the full DORT-focused response, and the reduced DORT-focused response are evaluated from the same scene data. This comparison distinguishes the benefit of singular-vector weighting from simple unweighted state combination and isolates the effect of discarding low-importance measurements.

F. Assumptions, Reproducibility, and Limitations of the Model

The simulation contains several deliberate approximations that define the scope of the conclusions.

First, the CST field data characterize each state at the 4.5 GHz reference frequency. The full 4–5 GHz cavity response is synthetic but anchored to the CST-derived complex state weights. The model therefore tests the signal-processing consequences of plausible wideband state diversity; it does not replace measured vector-network-analyzer calibration of the physical cavity at every frequency and stirrer state.

Second, target amplitudes are based on radar-equation scaling and a simplified bistatic or monostatic-equivalent geometry. The targets and clutter components are represented as point-like coherent scatterers. Extended-target scattering, polarization-dependent RCS, shadowing, and mutual coupling between the scene and the radar front end are not included.

Third, clutter and external multipath are represented by a limited number of additional coherent paths rather than by a fully statistical land, sea, urban, or indoor channel model. This is sufficient to test mode competition and ghost-range formation in a controlled way, but it cannot establish performance in a particular operational environment.

Fourth, the target and environment are assumed to remain coherent while the required frequency-state samples are acquired. Doppler, micro-Doppler, target acceleration, and time-varying interference are not included in the present scenarios. A mechanical stirrer is therefore appropriate for the current concept study, but faster electronic or electromechanical state control would be required for rapidly changing scenes.

Fifth, the calibrated cavity states are assumed to be repeatable. Temperature drift, mechanical positioning error, insertion loss, phase instability, and calibration aging are not explicitly perturbed in the baseline simulations. These effects should be addressed through calibration-error sensitivity studies and measured repeatability tests.

Finally, the reported processing-load metric counts frequency-state samples rather than processor operations, latency, transmitted energy, or dwell time. It is a transparent measure of measurement-set reduction, but the eventual system-level benefit will depend on waveform generation, state-switching speed, receiver architecture, and implementation of the SVD and range-processing stages.

Within these boundaries, the model is suitable for the present purpose: it tests whether physically anchored cavity-state

diversity can create a structured frequency-state response, whether DORT can identify the dominant coherent mode, and whether a reduced measurement subset can preserve the target range across representative link-budget conditions.

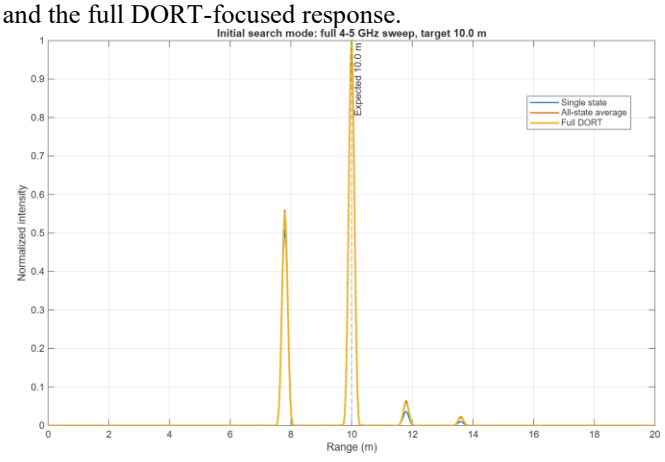
VI. RESULTS AND DISCUSSION

This section evaluates whether the simulated frequency-state measurements support the three central claims of the proposed architecture: first, that the calibrated cavity states provide a structured radar measurement basis; second, that DORT processing can extract a target-coupled mode and recover the target range; and third, that a reduced set of states and frequencies can preserve the useful response. The four scenarios defined in Table III are processed using the same CST-derived state anchors, synthetic wideband cavity model, target and clutter realization, regularized calibration, and DORT procedure. Full and reduced results are therefore compared on a like-for-like basis.

The electromagnetic field and angular-pattern results in Section III establish that the stirrer positions produce different aperture states. The present section concentrates on the radar consequences of that diversity. Results are interpreted as evidence of internal feasibility rather than as measured detection limits, because the detailed 4–5 GHz cavity transfer functions and the long-range scene are simulated rather than experimentally measured.

A. Full-Search Range Estimation

The full-search mode uses all available frequency samples and all seven cavity states. For each scenario, the calibrated frequency-state matrix is decomposed and projected onto the leading right singular vector before frequency-to-range transformation. A useful first comparison is therefore between a single-state response, an unweighted all-state combination, and the full DORT-focused response.



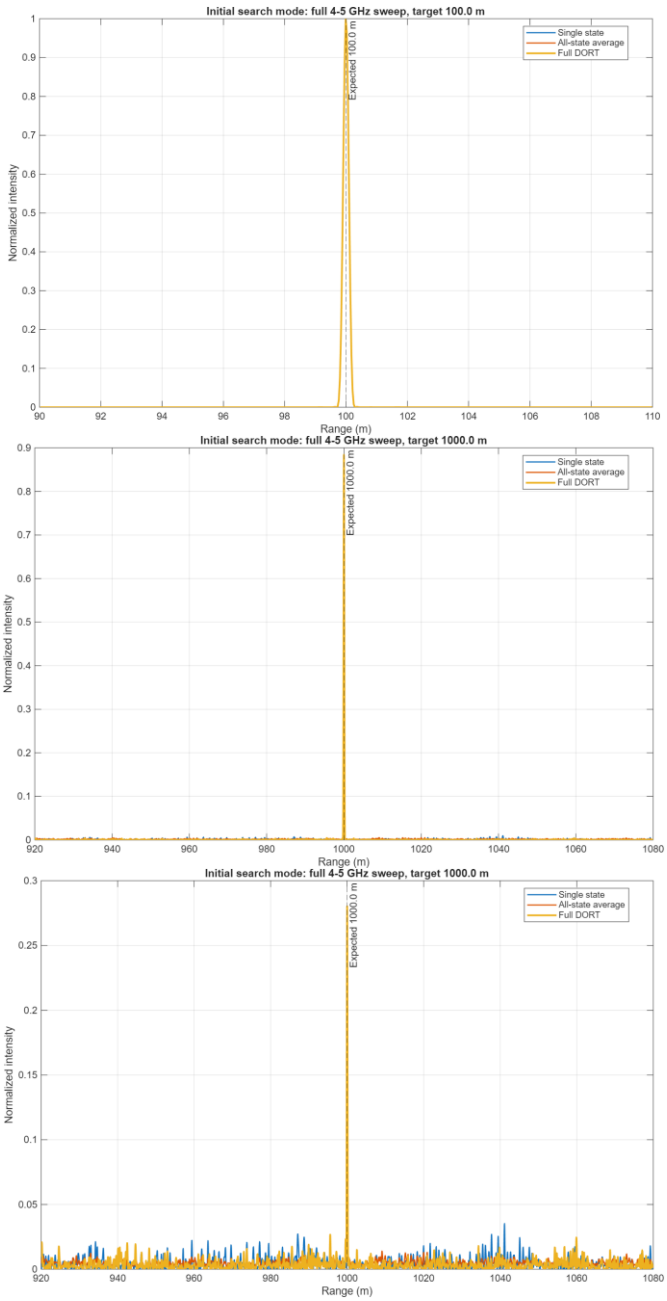


Fig. 7. Full-search range responses for the four representative simulation scenarios: (a) 10 m laboratory-scale target with 1 m² RCS; (b) 100 m outdoor target with 1 m² RCS; (c) 1 km target with 1 m² RCS; and (d) 1 km reduced-RCS stress case with 0.1 m² RCS. Each panel compares the response from a representative single cavity state, the unweighted all-state combination, and the full DORT-focused response obtained using all available frequencies and seven cavity states. The vertical marker indicates the simulated target range. The profiles are normalized independently to emphasize peak location and surrounding clutter or sidelobe structure.

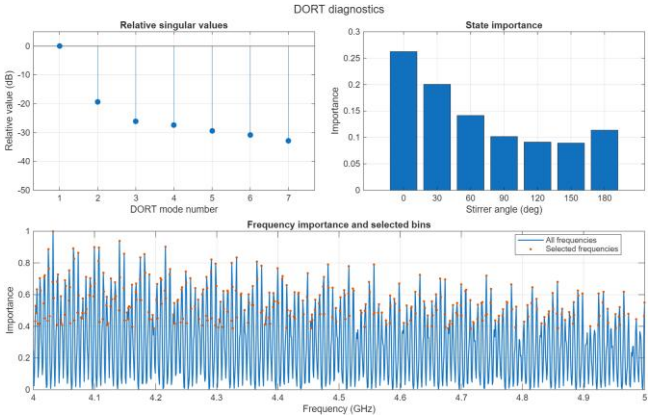
In Scenario A, the full DORT response peaks at 10.00 m, coincident with the known target range. Additional weaker peaks are produced by the deliberately introduced clutter scatterers, but the calibrated target response remains the strongest coherent feature. The result demonstrates that DORT is not merely averaging the seven states: it forms the complex state combination associated with the dominant coherent return. The same processing recovers 99.99 m in Scenario B and 999.99 m in Scenarios C and D. These estimates differ from the

specified ranges by no more than 0.01 m. This small numerical offset reflects interpolation of the zero-padded range grid and should not be interpreted as centimetric physical resolution; the nominal range resolution remains approximately 0.15 m, as established by the 1 GHz occupied bandwidth in (32). The appropriate result is therefore that the correct range bin and main-lobe location are preserved across the four representative link budgets.

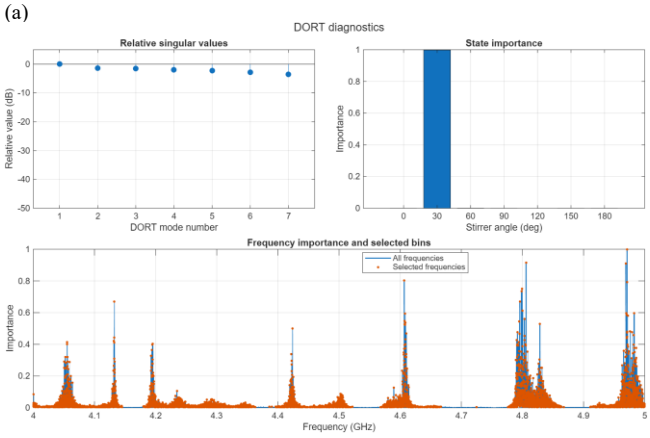
The state-resolved range maps provide an additional check. At 10 and 100 m, the target forms a vertical response at the expected range across several cavity states, while the relative intensity changes with stirrer angle. This confirms that the states provide different target couplings rather than seven identical copies of the same measurement. At 1 km, the target line remains visible, but the state-to-state contrast is less uniform, and the background contribution is more apparent, particularly in the reduced-RCS stress case.

B. DORT Modal Structure and Importance Measures

The singular-value spectrum and the associated state- and frequency-importance functions explain how the DORT result is formed. In Scenarios A and B, the first singular value is separated from the second by approximately 20 dB. The leading right singular vector distributes importance over several stirrer states, with the strongest contributions arising from a subset rather than from uniform weighting. This behavior is consistent with a dominant coherent target-coupled component embedded in weaker clutter and residual terms.



(a)



(b)

Fig. 8. Representative DORT diagnostics for the (a) 100 m outdoor scenario and the (b) 1 km reduced-RCS stress case. The panels compare the relative singular-value spectrum, leading-mode cavity-state importance, and leading-mode frequency importance. The 100 m case exhibits a clearly separated dominant mode with contributions distributed over several cavity states, whereas the stress case shows weaker singular-value separation, concentration of the state weighting around one stirrer position, and a more fragmented set of useful frequency samples. Markers on the frequency-importance curves identify the samples retained for reduced interrogation.

The frequency-importance curves are strongly structured across the 4–5 GHz band. Peaks occur in multiple separated sub-bands rather than being uniformly distributed over frequency. The selected bins therefore follow the target-coupled spectral structure generated by the combined cavity and scene response. This provides a physical basis for frequency reduction: the algorithm retains samples that contribute most strongly to the focused mode rather than applying a uniformly decimated sweep.

The long-range cases require more cautious interpretation. In Scenarios C and D, the singular values are clustered within only a few decibels and the state-importance function becomes strongly concentrated around one state. The range peak remains recoverable, but the evidence for a well-separated rank-one mode is weaker than in the 10 and 100 m cases. This is an important result rather than a failure of the study: it shows that correct range recovery alone is insufficient to establish a robust DORT mode. A practical implementation should use the singular-value gap, leading-mode energy fraction, or a related confidence statistic before changing from full search to reduced interrogation.

The implementation retains a minimum of three states even when the leading singular vector is dominated by one state. This prevents the reduced measurement from collapsing to a single-state radar, but it also means that the number of retained states is partly constrained by the selection rule. The final experimental study should therefore compare threshold-based selection with fixed-cardinality, cumulative-energy, and condition-number-based alternatives.

C. Focused Reduced Interrogation

The principal result is the comparison between the full DORT profile and the profile reconstructed from the DORT-selected frequency and state subsets. Table IV summarizes the quantitative outcomes. Scenarios A and B retain five of the seven states and 358 of 1024 frequency samples. The resulting measurement-set fraction is approximately 25%, corresponding to a 75% reduction. Scenarios C and D retain three states and 5734 of 16384 frequency samples, giving a measurement-set fraction of approximately 15% and an 85% reduction.

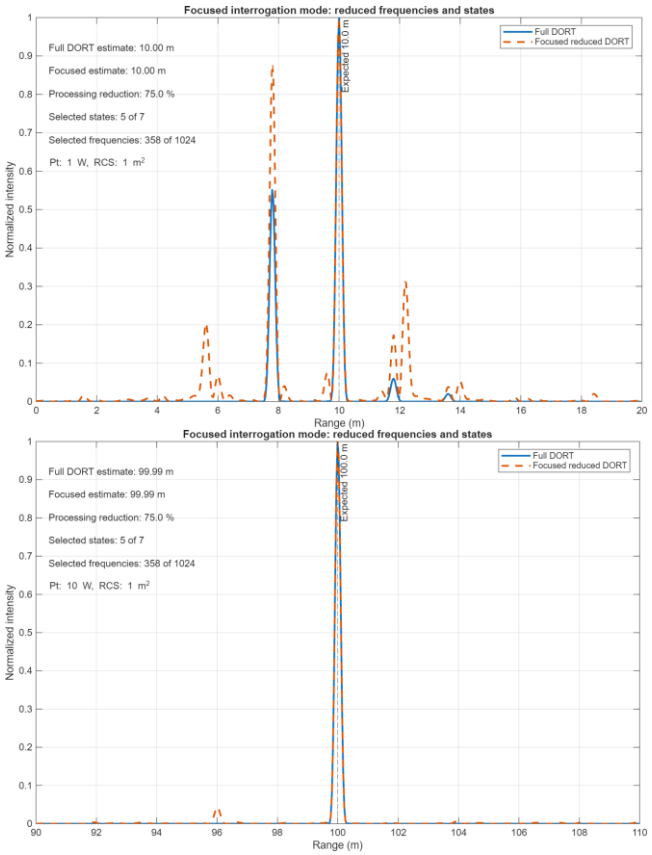
TABLE IV
SUMMARY OF FULL AND REDUCED DORT RESULTS

Scenario	Target range (m)	Estimated range, full / reduced (m)	Retained subset	Reduction
A	10	10.00 / 10.00	5/7 states358/1024 frequency bins	75.0%
B	100	99.99 / 99.99	5/7 states358/1024 frequency bins	75.0%
C	1000	999.99 / 999.99	3/7 states5734/16384 frequency bins	85.0%

Scenario	Target range (m)	Estimated range, full / reduced (m)	Retained subset	Reduction
D	1000	999.99 / 999.99	3/7 states5734/16384 frequency bins	85.0%

In all four scenarios, the reduced profile peaks at the same range as the full profile. The result demonstrates that the target information is not distributed uniformly across the complete frequency-state matrix. For the simulated scenes, the dominant range response can be reconstructed from a target-dependent subset selected from the leading DORT mode.

The cost of reduction is visible in the profile shape. Scenario A shows increased secondary peaks associated with the clutter returns when the reduced subset is used. Scenario B remains comparatively clean. Scenario C preserves a sharp target peak with low residual background, whereas Scenario D exhibits a noticeably higher and more irregular sidelobe and noise floor.



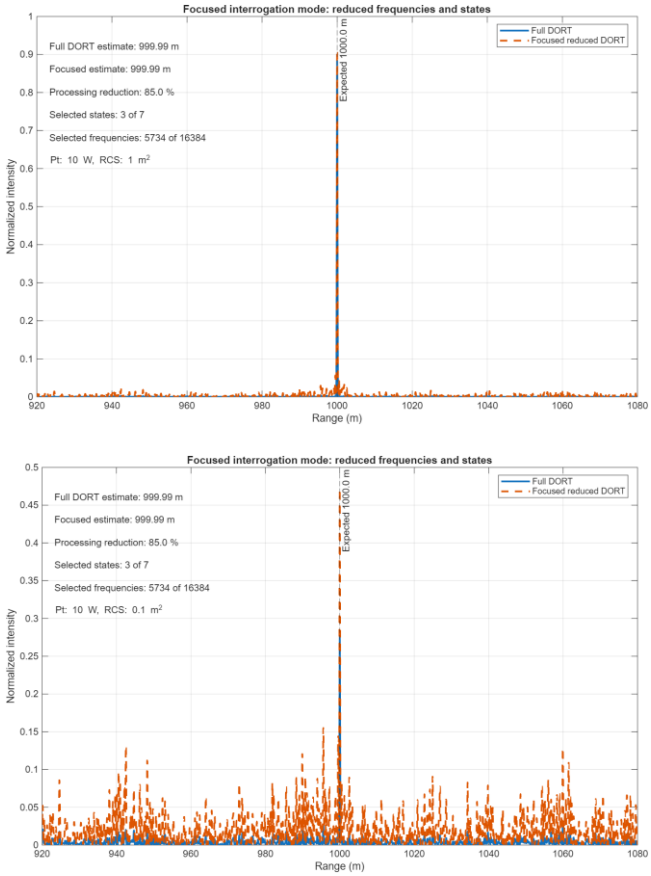


Fig. 9. Comparison of full and reduced DORT-focused range profiles for the four representative scenarios: (a) 10 m laboratory-scale target; (b) 100 m outdoor target; (c) 1 km target with 1 m² RCS; and (d) 1 km reduced-RCS stress case with 0.1 m² RCS. The full response uses all available frequency samples and seven cavity states, whereas the reduced response uses the DORT-selected frequency and state subsets. The dashed vertical marker indicates the simulated target range. Each panel is normalized independently to emphasize preservation of the target peak and changes in sidelobe or background structure.

The stress case therefore preserves the peak location but not the same degree of robustness or dynamic range as the full measurement. Reduced interrogation preserves the estimated range in these examples, but it does not guarantee unchanged sidelobe performance, detection probability, or false-alarm behavior.

The reduction percentages in Table IV count processed frequency-state samples, as defined in (29) and (30). They are not direct measurements of execution time, transmitted energy, dwell time, or hardware switching latency. Nevertheless, the result establishes a first-order selection benefit that could translate into one or more of those system-level savings, depending on the eventual implementation.

D. Frequency- and State-Resolved Target Structure

The range-frequency maps show where the focused target response is supported within the operating band. In the 10 and 100 m cases, a continuous ridge is visible around the expected target range over a broad central portion of the band, with weaker range-dependent structure associated with clutter and transform sidelobes. The maps demonstrate that the target response is coherent over frequency but not equally strong at every frequency.

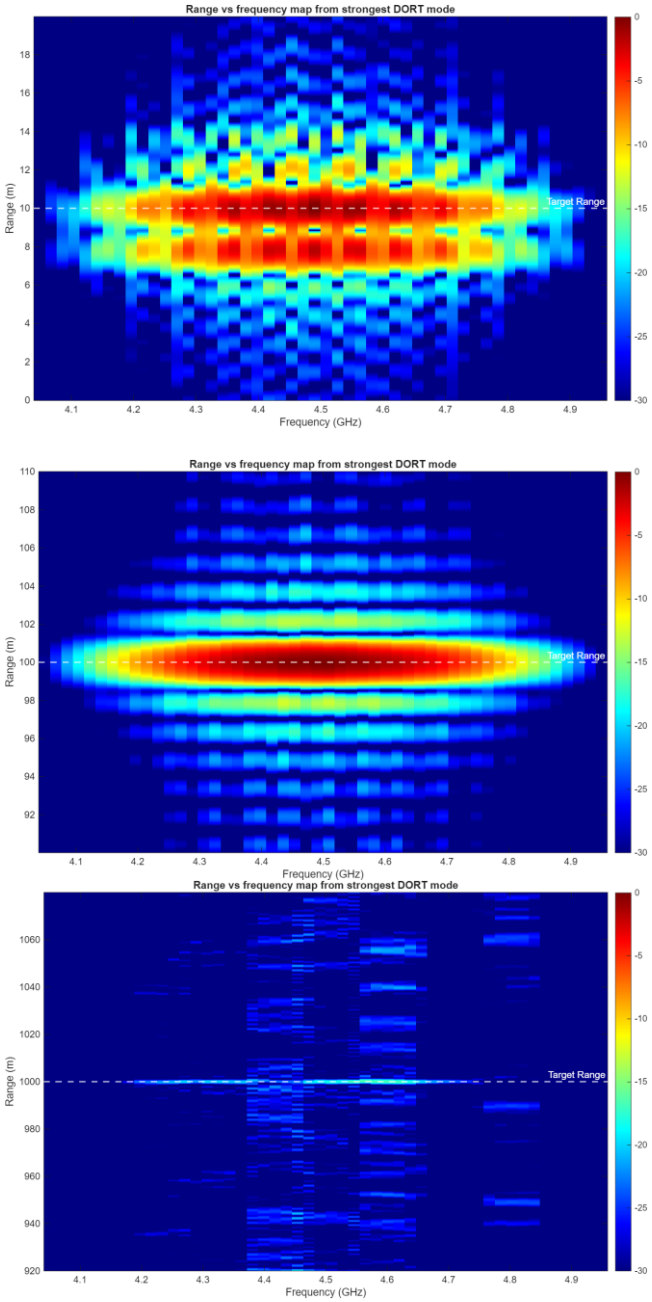


Fig. 10. Range–frequency magnitude maps obtained from the dominant DORT mode for: (a) the 10 m laboratory-scale (b) 100 m outdoor scenario and (c) the 1 km reduced-RCS stress case. The dashed horizontal line indicates the simulated target range. The short-range case exhibits a coherent target ridge over a substantial portion of the 4–5 GHz band, whereas the stress case shows a more fragmented frequency-dependent response and greater competition from residual background structure. The maps are normalized independently and displayed over the same dynamic range.

In the 1 km stress case, the target ridge is still identifiable near 1000 m, but the useful response is concentrated into more fragmented frequency regions and competes with additional range-frequency structure. This result supports adaptive spectral selection, but it also shows why the selected bins cannot be assumed to remain optimal indefinitely. Changes in target aspect, external multipath, interference occupancy, or calibration may alter the useful sub-bands; a practical radar would therefore need to refresh the full or expanded measurement periodically.

The state-resolved maps lead to the same conclusion in the cavity-state dimension. The selected-state maps retain the vertical target response at the correct range, indicating that the algorithm has not chosen states arbitrarily. However, the dominance of a single state in the long-range cases suggests that reduced-state operation should be confidence-controlled. A minimum-state constraint, periodic full-state revisit, or tracking of the right singular vector over time would reduce the risk of over-specializing the radar to a noisy instantaneous estimate.

E. Preservation of the DORT-Weighted Angular Structure

Section III showed that the individual cavity states produce related but measurably different angular patterns. The DORT weights combine those physical states into an effective target-coupled pattern. The full-state and reduced-state DORT-weighted cuts remain broadly similar in the representative results, indicating that the selected subset preserves much of the angular structure associated with the dominant mode.

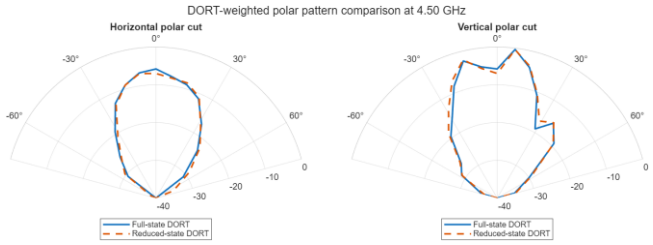


Fig. 11. Full-state and reduced-state DORT-weighted angular-pattern cuts at 4.5 GHz for a representative simulation scenario: (a) horizontal cut and (b) vertical cut. The full result combines all seven cavity states using the dominant DORT state vector, whereas the reduced result uses only the selected cavity-state subset. The broadly similar main-beam structure indicates that the reduced state set preserves much of the angular response associated with the dominant target-coupled mode, although local null and sidelobe differences remain.

This result should be interpreted as computational state focusing rather than conventional phased-array beam steering. The horn aperture still determines the broad physical radiation envelope, and the present simulation does not demonstrate measured retransmission of a physically focused time-reversed field. The result demonstrated is that the frequency-state data can be weighted to emphasize the dominant target-coupled response while using fewer cavity states.

F. Cross-Scenario Discussion and Strength of the Evidence

Taken together, the four scenarios support the internal feasibility of cavity-state coded radar. The CST-derived fields provide nonidentical electromagnetic states; the calibrated frequency-state matrices contain recoverable range structure; DORT forms a target-focused response; and selected subsets preserve the correct target range while reducing the number of processed samples by 75–85%. The results also show a meaningful progression with link-budget difficulty. At 10 and 100 m, the singular structure is clear, and the reduced profiles remain well behaved. At 1 km, the target range remains recoverable, but modal separation weakens and the stress case exhibits a substantial increase in background structure.

The results do not yet establish that cavity-state coding outperforms a conventional radar using the same bandwidth and energy. A stronger causal comparison should include at least

three ablations: DORT-selected subsets versus randomly selected subsets of equal size; DORT weighting versus power-only or uniform weighting; and the seven-state system versus a single fixed cavity state. These comparisons would test whether the observed reduction follows specifically from the calibrated DORT selection rather than from redundancy in the simulated data.

These results establish internal electromagnetic and algorithmic feasibility but not measured operational performance. The experimental, environmental, and dynamic-scene validation required to test the concept physically is considered in Section VII.

VII. EXTENSIONS, LIMITATIONS, AND EXPERIMENTAL VALIDATION PATHWAY

The results in Section VI support the feasibility of cavity-state coding as a calibrated radar-diversity mechanism, but they do not establish the performance of a complete operational radar. Section V identified the principal modelling assumptions; the present section considers their practical consequences and sets out the steps required to progress from simulation-led feasibility to measured radar validation. Particular attention is given to calibration stability, external multipath, extension to multiple targets, moving-target coherence, tracking, and the additional information contained in the singular vectors.

A. Calibration Repeatability and Wideband Experimental Validation

The highest-priority validation step is direct measurement of the complex cavity-state response over the complete 4-5 GHz operating band. In the present model, CST provides state-dependent field information at 4.5 GHz, while the detailed wideband modal response is synthetic. A physical implementation should therefore establish a measured dictionary for every frequency and cavity state using a vector network analyser. Two complementary measurements are desirable: an RF transfer-function measurement of the cavity and feed, and a radiated complex calibration using a fixed reference antenna or near-field probe. The second measurement is especially important because it includes the state-dependent coupling from the cavity through the horn into the external field.

The calibration should be repeated over multiple stirrer cycles and, where possible, over temperature, input power, vibration, and elapsed time. Let $\mathbf{H}_{\mathrm{c}}^{(\mathrm{ref})}$ denote the reference frequency-state dictionary and $\mathbf{H}_{\mathrm{c}}^{(q)}$ the dictionary obtained during repeat measurement q. A normalized calibration-drift metric may be written as

$$\epsilon_{\mathrm{cal}}^{(q)} = \frac{\left\|\mathbf{H}_{\mathrm{c}}^{(q)} - \mathbf{H}_{\mathrm{c}}^{(\mathrm{ref})}\right\|_F^2}{\left\|\mathbf{H}_{\mathrm{c}}^{(\mathrm{ref})}\right\|_F^2} \tag{40}$$

This metric should be reported together with pairwise state correlations, phase drift, amplitude drift, and the repeatability of the singular-value spectrum. Calibration-error sensitivity should then be introduced deliberately in the radar model to determine how much dictionary mismatch can be tolerated before the range estimate, dominant mode, or selected state set becomes unstable. The regularization parameter should also be reassessed from measured noise and cavity-null statistics rather than selected only from simulation convenience.

Measured target validation should proceed from a controlled short-range geometry to outdoor and extended-range cases. At each stage, the measured all-state response, full DORT response, and reduced-interrogation response should be compared using the same range-error, singular-value, and processing-load metrics employed in Section VI. The important question is not simply whether a target peak is visible, but whether the measured frequency-state structure supports a repeatable target-coupled mode and whether the reduced state/frequency set remains valid across repeated observations.

B. External Multipath, Clutter, and Interference

The cavity produces controlled internal multipath that is part of the calibrated front end. Buildings, walls, the ground, vehicles, and other external objects produce additional propagation paths after radiation. These paths are not automatically detrimental. If the environment is stable and sufficiently characterized, they may provide additional viewing diversity and an enlarged effective aperture, consistent with the broader time-reversal radar literature. However, a strong static reflector can also create a coherent singular mode that is larger than the desired target mode, and indirect paths may produce ghost ranges or mode mixing.

A practical system should therefore distinguish between the front-end calibration dictionary and the environmental background response. If $\mathbf{Z}_{\mathrm{bg}}$ is a calibrated empty-scene or background matrix and $\mathbf{Z}_{\mathrm{scene}}$ is the matrix measured with the target scene present, a first-order differential matrix is

$$\Delta\mathbf{Z} = \mathbf{Z}_{\mathrm{scene}} - \mathbf{Z}_{\mathrm{bg}} \tag{41}$$

DORT can then be applied to either the differential matrix or to a matrix projected away from a learned static-clutter subspace. Range gating, Doppler filtering, repeated background updates, and examination of several singular modes should be used together; the largest singular value should not be assumed automatically to represent the desired target.

External-multipath validation should be staged. An initial experiment can introduce one known metallic reflector to create a controlled indirect path. A second stage can use a static indoor or building-rich environment and compare processing with and without background subtraction. Later experiments should include moving clutter, intermittent interference, and deliberately contaminated frequency regions. Such tests would determine whether frequency-state selection genuinely provides resilience when parts of the measurement space are unavailable, rather than only reducing the number of processed samples in an otherwise clean simulation.

C. Extension to Multiple Targets

The principal contribution of the present paper is the introduction and single-target feasibility assessment of cavity-state coded radar. Multiple-target processing is therefore treated as an extension rather than as a demonstrated capability. In a scene containing several targets, the calibrated frequency-state matrix may contain several significant singular modes. A natural first approach is to form a focused spectrum for each

retained mode by projecting the matrix onto the corresponding right singular vector, then examine the associated range and angular response.

A one-to-one correspondence between singular modes and physical targets cannot, however, be assumed. A single extended target can contain several scattering centers and generate more than one mode, while two coherent targets can occupy the same subspace. A strong target may also dominate several of the leading modes, leaving a weaker target mixed with sidelobes, clutter, or residual model error. Reliable separation will therefore depend on relative radar cross-section, range and angular spacing, state-dependent coupling, clutter level, calibration quality, and the effective rank of the measured cavity-state dictionary.

Exploratory development simulations have extended the model to a CST-derived frequency-dependent angular dictionary $B_s(f,\theta)$ and a range-angle matched representation. These tests show a credible route to locating the dominant target in a multi-target scene, but they also show that a weaker target is not necessarily isolated as a clean independent DORT mode. This observation is useful because it identifies the correct next research questions without changing the scope of the present paper. A systematic follow-on study should begin with two comparable targets that are clearly separated in range, then examine equal-range/different-angle cases, unequal target strengths, adjacent range cells, and controlled clutter.

Future multiple-target processing may require range or angular gating, clutter-subspace projection, mode deflation, MUSIC-like subspace methods, or joint range-angle-mode association. Mode continuity across repeated observations may also provide a useful association feature through correlation of the right singular vectors. These topics are sufficiently substantial to form a separate investigation and are not included among the performance claims of the present work.

D. Moving Targets and a Search-to-Track Architecture

Target motion introduces a second time scale. The current frequency-state matrix assumes that the scene remains coherent while the required frequency and cavity-state samples are acquired. For a moving target, the data can be extended over slow time to form

$$\mathcal{Z}_{n,m,\ell} = Z(f_n, s_m, t_\ell) \tag{42}$$

where t_ℓ denotes the slow-time index. The duration of one frequency-state acquisition, T_{seq}, should remain small compared with the channel coherence time T_{c},

$$T_{\mathrm{seq}} \ll T_{\mathrm{c}} \tag{43}$$

If this condition is not satisfied, target motion can introduce phase variation during the state sequence that is confused with frequency- or state-dependent structure, reducing singular-mode concentration and time-reversal focusing. The moving-target time-reversal literature shows that channel variation must be incorporated into the processing model rather than ignored [20].

A credible cavity-state tracking architecture would separate acquisition from tracking. An initial full frequency-state search would provide a range-angle detection and initiate a track. The predicted target state would then define a local range-angle gate for subsequent DORT measurements. Within that gate, a reduced set of frequencies and cavity states could be used to increase the update rate. The resulting range, angle, Doppler, mode strength, and state-signature measurements could be supplied to a conventional tracking filter. Periodic full-dictionary measurements would refresh the selected mode, check the calibration residual, search for new targets, and recover from maneuvers or missed detections.

The tracker itself is not a contribution of the present paper. Kalman, extended-Kalman, unscented-Kalman, or interacting-multiple-model filters could be used depending on the motion model. The distinctive cavity-state contribution lies upstream: the provision of calibrated DORT-derived measurements and a reduced-interrogation revisit mode. Prediction-gated processing is especially attractive because it can prevent an angular sidelobe or competing coherent mode from being selected when the available angular dictionary is restricted.

An illustrative internal simulation has demonstrated the mechanics of this search-to-track loop using initialized, prediction-gated DORT range-angle detections and a linear Kalman filter. The example is not reported as a validated tracking result because track initiation, data association, false tracks, missed detections, target crossings, calibration drift, and time-varying propagation were not evaluated. It nevertheless provides a practical blueprint for a follow-on paper centered on dynamic scenes and reduced-revisit tracking.

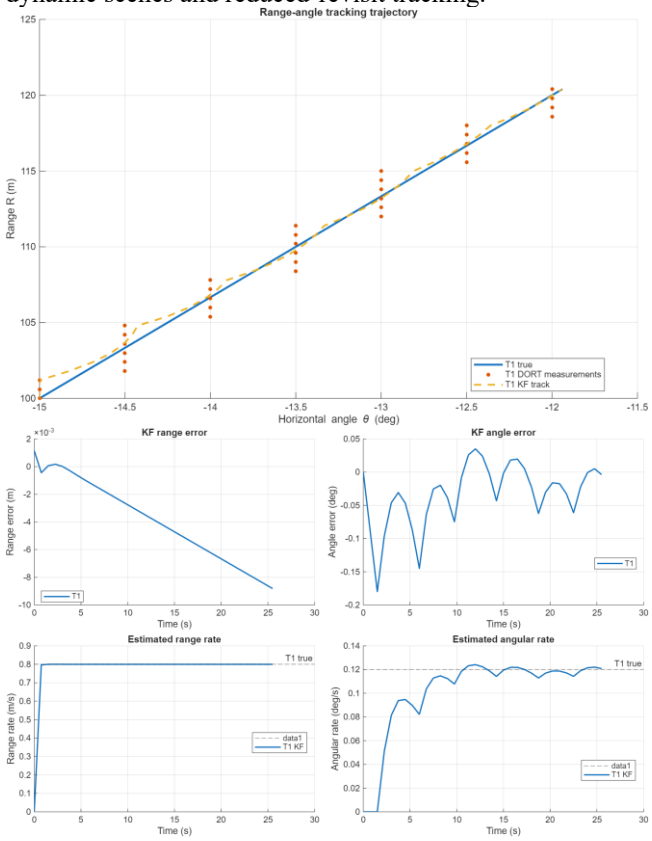


Fig. 12. Illustrative single-target range-angle tracking trajectory. The plot shows the true trajectory, DORT-derived measurements, and a prediction-gated filtered track. It is included only as a proof-of-principle indication of how repeated cavity-state measurements could support a conventional tracker; it is not part of the validated performance claims of this paper.

The reduced-interrogation result may therefore have a second benefit beyond reducing processed sample count: after acquisition, fewer frequency-state samples may shorten the revisit interval and improve the feasibility of tracking. This potential advantage cannot be quantified until waveform duration, state-switching time, receiver latency, and processing time are represented explicitly. Mechanical stirring is suitable for static proof-of-concept measurements, but rapidly moving targets will require substantially faster electronic or electromechanical state control.

E. Target Signatures and Higher-Dimensional Processing

The SVD contains information beyond the dominant range response. In the present formulation, the columns of $\mathbf{U}$ describe the frequency-domain structure of the scattering modes, the columns of $\mathbf{V}$ describe their cavity-state coupling, and the singular values describe their relative strength. These quantities may provide complementary target features: spectral resonances and phase structure in $\mathbf{U}$, electromagnetic-state signatures in $\mathbf{V}$, and scattering complexity or effective rank in $\mathbf{\Sigma}$. Ratios between singular values, the stability of the state vector over aspect, and the distribution of frequency importance may therefore support confidence scoring or target classification.

The role of $\mathbf{U}$ should nevertheless be stated carefully. A single frequency-state matrix does not contain a conventional micro-Doppler history, because micro-Doppler is a slow-time phenomenon produced by target vibration, rotation, or articulated motion [31]. Micro-Doppler analysis would require repeated frequency-state measurements. For mode k, a time-varying focused spectrum could be formed as

$$\mathbf{p}_k(t_\ell) = \mathbf{Z}(t_\ell)\,\mathbf{v}_k^*(t_\ell) \tag{44}$$

followed by range selection and time-frequency analysis of the resulting slow-time signal. The short-time Fourier transform provides the natural first representation for nonstationary Doppler signatures. Wavelet transforms may offer better localization for transient or multiscale motion, while wavelet scattering provides a possible route to deformation-stable multiscale features for classification [32].

A richer future model could therefore treat the data as a frequency-state-slow-time tensor and compare matrix SVD applied dwell by dwell with tensor decompositions that preserve coupling among frequency, cavity state, and slow time. This could reveal whether cavity-state coding adds useful discrimination to conventional range-Doppler or micro-Doppler features. At present, these are research opportunities rather than demonstrated capabilities and should not be interpreted as results of the static simulations reported here.

F. Faster State Control and Cognitive Operation

Mechanical stirring provides a clear and reproducible proof-of-concept mechanism, but it is unlikely to provide the switching speed required for agile radar operation. Faster implementations could use switched metallic perturbations, PIN diodes, varactors, RF MEMS, tunable materials, or electronically controlled meta-surface boundaries. The relevant design objective is not simply maximum switching speed. The states must also remain sufficiently distinct, radiatively efficient, repeatable, and calibratable over the operating band.

The state- and frequency-importance measures provide a natural input to a cognitive radar control loop. A future controller could combine spectrum occupancy, interference estimates, target-mode strength, calibration uncertainty, and switching cost when selecting the next measurement set. The radar could perform a broad search, identify a target-coupled mode, avoid contaminated frequencies, retain the most informative cavity states, and periodically re-explore the wider state space to prevent model lock-in. Such a controller would convert the reduced-interrogation method from a post-processing demonstration into an adaptive sensing policy.

The optimization objective should include more than sample count. Relevant costs include transmitted energy, dwell time, state-switching latency, receiver dynamic range, calibration age, spectral occupancy, and the condition number of the selected state dictionary. A state with high singular-vector weight may still be undesirable if it lies near a deep cavity null, switches slowly, or occupies a prohibited frequency region. Cognitive selection should therefore be constrained by both electromagnetic usefulness and system-level feasibility.

G. Recommended Validation Sequence and Scope of Claims

A staged validation program is recommended so that failures can be attributed to the cavity hardware, calibration, propagation environment, or signal processing rather than being confounded in one end-to-end experiment.

TABLE V
Recommended Experimental and Algorithmic Validation Sequence

Stage	Primary objective	Principal outputs
Wideband state calibration	Measure the complex 4-5 GHz response of every state and quantify repeatability	Measured dictionary, state correlation, drift, null statistics, conditioning
Static single-target validation	Reproduce the full and reduced DORT range results in a controlled geometry	Range error, singular-value spectrum, state/frequency importance, repeatability
Clutter, multipath, and interference	Test background subtraction, clutter-subspace rejection, and frequency avoidance	Mode competition, ghost suppression, robustness to contaminated bins
Multiple-target follow-on study	Establish when distinct targets generate separable range-angle or DORT representations	Strong/weak target behavior, mode mixing, association criteria, resolvability limits
Dynamic-target follow-on study	Quantify coherence loss and evaluate prediction-gated reduced revisits	Update rate, DORT measurement quality, mode continuity, tracking robustness
Faster state control and cognitive selection	Demonstrate adaptive state/frequency selection with practical switching	Latency, energy, occupancy, recalibration rate, closed-loop benefit

The claims of the present paper should remain limited to simulation-led feasibility. The results show that a CST-

anchored state basis and a plausible wideband cavity model can produce a structured frequency-state response, that DORT can recover the modelled target range, and that a reduced measurement subset can preserve that estimate in the representative cases examined. They do not establish probability of detection, false-alarm performance, operational interference rejection, low-probability-of-intercept performance, multi-target separation, real-time tracking, or target classification. Those capabilities require the measured validation sequence above.

Within this scope, the unresolved issues are constructive rather than fatal. They define a clear progression from a static mechanically stirred prototype to measured wideband calibration, controlled radar trials, dynamic and multi-target processing, and ultimately faster adaptive cavity-state control. The central research question for the next stage is therefore not whether the cavity produces complexity, but whether that complexity remains repeatable, sufficiently independent, and informative under real radar operating conditions.

VIII. CONCLUSION

This paper has introduced cavity-state coded radar, a radar architecture in which a reconfigurable reverberant cavity is treated as a calibrated electromagnetic state generator rather than solely as a feed structure. By sampling the scene jointly over frequency and cavity state, the received data are represented as a frequency-state matrix that can be regularized against a stored calibration dictionary and decomposed using DORT. The resulting singular structure provides a target-focused range response together with interpretable measures of cavity-state and frequency importance.

A hybrid CST/MATLAB framework was used to examine the physical and algorithmic plausibility of the concept. CST-derived fields at 4.5 GHz showed that the seven stirrer positions produce nonidentical near-field distributions, complex state weights, and angular radiation patterns. These electromagnetic data were used to anchor a synthetic wideband cavity model over 4-5 GHz, while MATLAB represented propagation, target returns, weak clutter, receiver noise, regularized time-reversal calibration, range processing, and DORT-based mode extraction. The study therefore connects a physically plausible reconfigurable front end to a coherent radar-processing formulation without claiming a completed operational radar demonstration.

Across representative 10 m, 100 m, and 1 km scenarios, including a reduced-RCS stress case, the full DORT response recovered the target in the correct range bin. Focused interrogation using DORT-selected cavity states and frequency samples preserved the full-search range estimate while reducing the processed frequency-state measurement, set by approximately 75% in the 10 m and 100 m cases and 85% in the 1 km cases. The reduced profiles did not always preserve the same sidelobe and background behavior, and the singular-value separation weakened in the long-range cases. These observations indicate that transition to reduced interrogation should be controlled by a confidence measure such as the singular-value gap, leading-mode energy fraction, calibration residual, or stability of the selected state vector.

The principal implication is that useful radar diversity may be generated through calibrated internal electromagnetic reconfiguration rather than only through additional RF channels, larger antenna arrays, or broader waveform sets. Cavity-state coded radar is not proposed as a direct replacement for phased-array radar; it occupies a different design trade-space in which hardware simplicity at the radiating aperture is exchanged for cavity design, state repeatability, calibration, and signal processing. In congested electromagnetic environments, the broad-search and focused-interrogation sequence could provide a route to retaining target-coupled frequency-state combinations while avoiding contaminated spectral regions or reducing the measurement burden for subsequent revisits.

The conclusions remain conditioned by the simulation-led nature of the study. The state-dependent electromagnetic anchors were derived from CST at one reference frequency, whereas the detailed 4-5 GHz cavity response was synthetic. Clutter and external multipath were represented in simplified form, the targets were stationary during each frequency-state acquisition, and mechanical repeatability, calibration drift, switching latency, and measured retransmission were not evaluated. The highest-priority next steps are therefore direct wideband measurement of every cavity state, repeatability and drift characterization, and controlled single-target experiments comparing full and reduced DORT processing. These should be followed by realistic clutter, multipath, and interference tests and by investigation of faster electronic or electromechanical state control.

Subject to those validation steps, the results establish cavity-state coding as a technically credible radar concept worthy of experimental investigation. The work shows that a reconfigurable cavity can create a calibrated electromagnetic state space, that DORT can extract and rank coherent target-coupled structure within that space, and that the resulting information can support focused interrogation with a substantially reduced measurement set. More broadly, the study suggests that calibrated electromagnetic state diversity may provide a useful new resource for adaptive radar sensing and resource management in complex and spectrally congested environments.

ACKNOWLEDGMENT

REFERENCES

[1] S. Haykin, “Cognitive radar: A way of the future,” IEEE Signal Process. Mag., vol. 23, no. 1, pp. 30–40, Jan. 2006, doi: 10.1109/MSP.2006.1593335.

[2] M. Labib, V. Marojevic, A. F. Martone, J. H. Reed, and A. I. Zaghloul, “Coexistence between communication and radar systems—A survey,” URSI Radio Sci. Bull., vol. 2017, no. 362, pp. 74–82, Sep. 2017.

[3] A. F. Martone and M. G. Amin, “A view on radar and communication systems coexistence and dual functionality in the era of spectrum sensing,” Digit. Signal Process., vol. 119, Art. no. 103135, Dec. 2021, doi: 10.1016/j.dsp.2021.103135.

[4] D. Cohen, K. V. Mishra, and Y. C. Eldar, “Spectrum sharing radar: Coexistence via Xampling,” IEEE Trans. Aerosp. Electron. Syst., vol. 54, no. 3, pp. 1279–1296, Jun. 2018, doi: 10.1109/TAES.2017.2780599.

[5] J. J. Lynch, "Low latency digital beamforming radar using aperture coding," IEEE Trans. Aerosp. Electron. Syst., vol. 52, no. 2, pp. 918–927, Apr. 2016, doi: 10.1109/TAES.2016.140944.

[6] R. S. P. Sankar and S. P. Chepuri, "Coded aperture radar imaging using reconfigurable intelligent surfaces," in Proc. IEEE 9th Int. Workshop Comput. Adv. Multi-Sensor Adaptive Process. (CAMSAP), 2023, pp. 171–175, doi: 10.1109/CAMSAP58249.2023.10403473.

[7] T. A. Sleasman, M. F. Imani, A. V. Diebold, M. Boyarsky, K. P. Trofatter, and D. R. Smith, "Implementation and characterization of a two-dimensional printed circuit dynamic metasurface aperture for computational microwave imaging," IEEE Trans. Antennas Propag., vol. 69, no. 4, pp. 2151–2164, Apr. 2021, doi: 10.1109/TAP.2020.3027188.

[8] M. García-Fernández, G. Alvarez-Narciandi, and O. Yurduseven, "Frequency-diverse metasurface antenna for computational through-wall imaging," in Proc. 17th Eur. Conf. Antennas Propag. (EuCAP), Florence, Italy, Mar. 2023, pp. 1–5, doi: 10.23919/EuCAP57121.2023.10133569.

[9] M. Fink, D. Cassereau, A. Derode, C. Prada, P. Roux, J.-L. Thomas, and F. Wu, "Time-reversed acoustics," Rep. Prog. Phys., vol. 63, no. 12, pp. 1933–1995, Dec. 2000, doi: 10.1088/0034-4885/63/12/202.

[10] C. Prada and M. Fink, "Eigenmodes of the time reversal operator: A solution to selective focusing in multiple-target media," Wave Motion, vol. 20, no. 2, pp. 151–163, Sep. 1994, doi: 10.1016/0165-2125(94)90039-6.

[11] C. Prada, S. Manneville, D. Spoliansky, and M. Fink, "Decomposition of the time reversal operator: Detection and selective focusing on two scatterers," J. Acoust. Soc. Amer., vol. 99, no. 4, pp. 2067–2076, Apr. 1996, doi: 10.1121/1.415393.

[12] C. Prada and J.-L. Thomas, "Experimental subwavelength localization of scatterers by decomposition of the time reversal operator interpreted as a covariance matrix," J. Acoust. Soc. Amer., vol. 114, no. 1, pp. 235–243, Jul. 2003, doi: 10.1121/1.1568759.

[13] H. Tortel, G. Micolau, and M. Saillard, "Decomposition of the time reversal operator for electromagnetic scattering," J. Electromagn. Waves Appl., vol. 13, no. 5, pp. 687–719, 1999, doi: 10.1163/156939399X01113.

[14] G. Micolau, M. Saillard, and P. Borderies, "DORT method as applied to ultrawideband signals for detection of buried objects," IEEE Trans. Geosci. Remote Sens., vol. 41, no. 8, pp. 1813–1820, Aug. 2003, doi: 10.1109/TGRS.2003.814139.

[15] A. J. Devaney, "Time reversal imaging of obscured targets from multistatic data," IEEE Trans. Antennas Propag., vol. 53, no. 5, pp. 1600–1610, May 2005, doi: 10.1109/TAP.2005.846723.

[16] D. Liu, G. Kang, L. Li, Y. Chen, S. Vasudevan, W. Joines, Q. H. Liu, J. Krolik, and L. Carin, "Electromagnetic time-reversal imaging of a target in a cluttered environment," IEEE Trans. Antennas Propag., vol. 53, no. 9, pp. 3058–3066, Sep. 2005, doi: 10.1109/TAP.2005.854563.

[17] Y. Jin and J. M. F. Moura, "Time-reversal detection using antenna arrays," IEEE Trans. Signal Process., vol. 57, no. 4, pp. 1396–1414, Apr. 2009, doi: 10.1109/TSP.2008.2010425.

[18] Y. Jin, J. M. F. Moura, and N. O'Donoughue, "Time reversal in multiple-input multiple-output radar," IEEE J. Sel. Topics Signal Process., vol. 4, no. 1, pp. 210–225, Feb. 2010, doi: 10.1109/JSTSP.2009.2038983.

[19] Z. Zhang, B. Chen, and M. Yang, "Time reversal detection in multistatic radar system," IEEE Access, vol. 8, pp. 93594–93611, 2020, doi: 10.1109/ACCESS.2020.2994976.

[20] Z. Zhang, B. Chen, and M. Yang, "Moving target detection based on time reversal in a multipath environment," IEEE Trans. Aerosp. Electron. Syst., vol. 57, no. 5, pp. 3221–3236, Oct. 2021, doi: 10.1109/TAES.2021.3074131.

[21] H. Lian, M. Yang, D. Zhou, and M. Liu, "Distributed MIMO radar target detection in multipath clutter environments with time reversal," IEEE Trans. Aerosp. Electron. Syst., vol. 61, no. 2, pp. 4907–4925, Apr. 2025, doi: 10.1109/TAES.2024.3510687.

[22] M. E. Yavuz and F. L. Teixeira, "Full time-domain DORT for ultrawideband electromagnetic fields in dispersive, random inhomogeneous media," IEEE Trans. Antennas Propag., vol. 54, no. 8, pp. 2305–2315, Aug. 2006, doi: 10.1109/TAP.2006.879196.

[23] M. E. Yavuz and F. L. Teixeira, "Space-frequency ultrawideband time-reversal imaging," IEEE Trans. Geosci. Remote Sens., vol. 46, no. 4, pp. 1115–1124, Apr. 2008, doi: 10.1109/TGRS.2008.915755.

[24] T. Sakamoto, "Stepped-frequency DORT imaging with singular value decomposition for a single-antenna ultrawideband radar in multi-path environments," arXiv:2110.06605, 2021.

[25] Blunt, Shannon & Mokole, Eric. (2016). Overview of radar waveform diversity. IEEE Aerospace and Electronic Systems Magazine. 31. 2-42. 10.1109/MAES.2016.160071.

[26] R. Serra et al., "Reverberation chambers a la carte: An overview of the different mode-stirring techniques," in IEEE Electromagnetic Compatibility Magazine, vol. 6, no. 1, pp. 63-78, First Quarter 2017, doi: 10.1109/MEMC.2017.7931986.

[27] Y. Rahmat-Samii, V. Galindo-Israel and R. Mittra, "A plane-polar approach for far-field construction from near-field measurements," in *IEEE Transactions on Antennas and Propagation*, vol. 28, no. 2, pp. 216-230, March 1980, doi: 10.1109/TAP.1980.1142316

[28] Weyl, Hermann (1911). "Über die asymptotische Verteilung der Eigenwerte". *Nachrichten der Königlichen Gesellschaft der Wissenschaften zu Göttingen*: 110–117.

[29] B. Rigling and M. Martorella, "Bistatic and Multistatic Radar Imaging," 2019 IEEE Radar Conference (RadarConf), Boston, MA, USA, 2019, pp. 1-223, doi: 10.1109/RADAR.2019.8835720.

[30] Radar Signal Analysis and Processing Using MATLAB Bassem R. Mahafza. Taylor & Francis, 2009.

[31] V. C. Chen, F. Li, S.-S. Ho, and H. Wechsler, "Micro-Doppler effect in radar: Phenomenon, model, and simulation study," *IEEE Trans. Aerosp. Electron. Syst.*, vol. 42, no. 1, pp. 2–21, Jan. 2006, doi: 10.1109/TAES.2006.1603402.

[32] S. Mallat, "Group invariant scattering," *Commun. Pure Appl. Math.*, vol. 65, no. 10, pp. 1331–1398, 2012, doi: 10.1002/cpa.21413.



Andrew J. Wileman received the B.Eng. degree (Hons.) in electronic engineering from the University of Nottingham, U.K., and the M.Sc. degree in digital communication systems from Loughborough University, U.K. In 2012, he joined the Integrated Vehicle Health Management (IVHM) Centre, Cranfield University, as a Ph.D. Researcher in prognostics for electronics/defense systems, sponsored by Thales, U.K., and Meggitt. He worked with the U.K. Ministry of Defence and other engineering companies within the U.K. He has lectured in electronics/communication engineering with further and higher education institutions for a number of years. He is currently working as a Research Associate in RF & Microwave Systems in the Electromagnetic Environment Hub (EMEHub) at Loughborough University.

Prof Nigel Seddon MBE received the B.Sc. (Hons) degree in Physics and Mathematics from the University of Reading (U.K.) in 1981, and the Ph.D. degree in Laser Physics from the

University of Hull (U.K.) in 1984, where his research focused on mercury bromide laser kinetics.
From 1984 to 2007, he worked at BAE Systems' Advanced Technology Centre, Filton, U.K., where his work there encompassed the development of high-power electromagnetic devices, antennas, metamaterials, plasma sources, pulsed power, and high-power laser technologies. From 2008 to 2023, he served as a technical specialist at MBDA UK Ltd, leading teams on Directed Energy Systems. Since 2023, he has worked as an independent consultant, providing advice on pulsed power and high-power electromagnetic technologies.